Inorg. Chem. **2009**, *48*, 1857−1870

Tuning Through-Bond Fe(III)/Fe(II) Coupling by Solvent Manipulation of a Central Ruthenium Redox Couple

Yu-Chen Lin,[†] Wei-Tin Chen,[†] Joe Tai,[†] Denny Su,[†] Sheng-Yi Huang,[†] Ingrid Lin,[†] Ju-Ling Lin,[†] Mandy M. Lee,[†] Mong Feng Chiou,[†] Yen-Hsiang Liu,[†] Ken-Shin Kwan,[†] Yuan-Jang Chen,*[,†] and Hsing-Yin Chen[‡]

Department of Chemistry, Fu Jen Catholic University, Taipei Hsien 24205, Taiwan, Republic of China, and Department of Medicinal and Applied Chemistry, Kaohsiung Medical University, Kaohsiung 24205, Taiwan, Republic of China

Received July 8, 2008

The relationships between the intervalence energy (E_{IT}) and the free energy difference (ΔG) that exists between the minima of redox isomers ($Fe^{II}-Ru^{III}/Fe^{III}-Ru^{II}$) for various heterobimetallic complexes $[(R\text{-}Fcpy)Ru(NH_3)_5]^{2+/3+}$ (R = H, ethyl, Br, actyl; Fcpy = (4-pyridyl)ferrocenyl; $Ru(NH_3)_5$ = pentaam(m)ineruthenium) were examined. The changes in ΔG for the complexes in various solvents were due to the effects of both solvent donicity and the substituents. The intervalence energy versus ΔG, $\Delta G \approx F\Delta E_{1/2}$ ($\Delta E_{1/2} = E_{1/2}(Fe^{III/II}) - E_{1/2}(Ru^{III/II})$), plots for the complexes in various solvents suggest a nuclear reorganization energy (λ) of ≈6000 cm^{-1} (Chen et al. *Inorg. Chem.* **2000**, *39*, 189). For $[(R\text{-}Fcpy)Ru(NH_3)_5]^{2+}$ and $[(et\text{-}Fcpy)Ru(NH_3)_4(py)]^{2+}$ ($Ru(NH_3)_4$ = *trans*-tetraam(m)ineruthenium; py = pyridine) in various solvents, the $E_{1/2}(Ru^{III/II})$ of rutheniumam(m)ine typically was less than the $E_{1/2}(Fe^{III/II})$ of the ferrocenyl moiety. However, the low-donicity solvents resulted in relatively large values of $E_{1/2}(Ru^{III/II})$ for $[(et\text{-}Fcpy)Ru(NH_3)_4(py)]^{2+/3+/4+}$. Under our unique solvent conditions, a dramatic end-to-end interaction was observed for the trimetal cation, $[(et\text{-}Fcpy)_2Ru(NH_3)_4]^{4+}$, in which the $[(et\text{-}Fcpy)_2Ru(NH_3)_4]^{4+}$ included a central *trans*-tetraam(m)ineruthenium(III) and a terminal Fe^{II}/Fe^{III} pair. In general, results of electrochemical studies of $[(et\text{-}Fcpy)_2Ru(NH_3)_4]^{2+}$ indicated both solvent-tunable $E_{1/2}(Ru^{III/II})$ (1 e^-) and solvent-insensitive $E_{1/2}(Fe^{III/II})$ (2 e^-) redox centers. However, in nitriles, two $E_{1/2}(Fe^{III/II})$ peaks were found with $\Delta E_{1/2}(Fe^{III/II} - Fe^{III/II})$ ranging between 83 and 108 mV at a terminal metal-to-metal distance of up to 15.6 Å. Furthermore, the bridging dπ orbital of the ruthenium center mediated efficient end-to-end interaction between the combinations of the terminal $Fe^{II}-Fe^{III}/Fe^{III}-Fe^{II}$ pair. To our knowledge, this is the first example of solvent-tunable end-to-end interactions in multimetal complexes.

Introduction

Multimetal mixed-valence complexes have been fundamentally important in understanding the properties of a wide range of thermal and photoinduced electron-transfer processes.[1−15] The matrix element, H_{DA}, between the donor (D) and acceptor (A) is a major factor in understanding the fundamental aspects of many electron-transfer processes, as it describes the potential efficiency of long-range electron transfer in biological systems and molecular wires.[1−18] The

* To whom correspondence should be addressed. E-mail: 054971@mail.fju.edu.tw.
† Fu Jen Catholic University.
‡ Kaohsiung Medical University.

(1) Hush, N. S. *Prog. Inorg. Chem.* **1967**, *8*, 391.
(2) Hush, N. S. *Electrochim. Acta* **1968**, *13*, 1005.
(3) Hush, N. S. *Coord. Chem. Rev.* **1985**, *64*, 135.
(4) Marcus, R. A.; Sutin, N. *Biochim. Biophys. Acta* **1985**, *811*, 265.
(5) Creutz, C.; Taube, H. *J. Am. Chem. Soc.* **1973**, *95*, 1086.
(6) Creutz, C. *Prog. Inorg. Chem.* **1983**, *30*, 1.
(7) Creutz, C.; Newton, M. D.; Sutin, N. *J. Photochem. Photobiol. A: Chem.* **1994**, *82*, 47.
(8) Newton, M. D. *Chem. Rev.* **1991**, *91*, 767.
(9) Newton, M. D. *Annu. Rev. Phys. Chem.* **1984**, *35*, 437.
(10) Richardson, D. E.; Taube, H. *Coord. Chem. Rev.* **1984**, *60*, 107.
(11) Nelsen, S. F.; Ismagilov, R. F.; Trieber, D. A. I. *Science* **1997**, *278*, 846.
(12) Demadis, K. D.; Hartdhorn, C. M.; Meyer, T. J. *Chem. Rev.* **2001**, *101*, 2655.
(13) Macatangay, A. V.; Endicott, J. F.; Song, X. *J. Phy. Chem. A* **1998**, *102*, 7537.
(14) Endicott, J. F.; Chen, Y.-J.; Xie, P. *Coord. Chem. Rev.* **2005**, *249*, 343.
(15) Crutchley, R. J. *Adv. Inorg. Chem.* **1994**, *41*, 273.
(16) Reimers, J. R.; Hush, N. S. *Chem. Phys.* **1996**, *208*, 177.
(17) Launay, J.-P. *Chem. Soc. Rev.* **2001**, *30*, 386.

10.1021/ic801271q CCC: $40.75
Published on Web 02/05/2009

well-known Mulliken−Hush expression for H_{DA} in a two-state system is given by[1,6,19,20]

$$H_{DA} = \frac{0.0205}{r} \times \sqrt{(\varepsilon_{max} \times \Delta\upsilon_{1/2} \times E_{IT})} \quad (1)$$

where ε_{max}, $\Delta\upsilon_{1/2}$, E_{IT}, and r are molar absorptivity (M^{-1} cm^{-1}), half-bandwidth (cm^{-1}), band maximum (cm^{-1}) of the intervalence band, and the distance between the donor and acceptor (Å), respectively. It is generally recognized that eq 1 underestimates H_{DA} when r is the distance separating the localized (diabatic) donor and acceptor centroids.[21,22] A review by Robin and Day classified mixed-valence complexes into three broad types:[23] class I, completely valence-trapped without coupling between the donor and acceptor (D/A); class II, valence-trapped with weak coupling between D and A; and class III, fully delocalized with very strong coupling between D and A. Most known mixed-valence systems are believed to fall into class II,[6,10,15] and complexes of the type $[\{Ru(NH_3)_5\}_2BL]^{n+}$ (BL = bridging ligand)[24−27] in which $H_{DA} < 300$ cm^{-1} have often been used to test the validity of the theories.[10,14−16] Mixed-valence complexes containing the biferrocenyl cation ($[Fc-BL-Fc]^+$, BL = bridging moiety) have also been very useful model systems for examining fundamental electron-transfer issues.[28−31] When only one of the centers of such a bimetallic complex is solvent-tunable,[32−36] the difference in the energies of the D/A states has been found to correlate with solvent donicity,[37] and such solvent control of the D/A properties can even reverse the donor and acceptor states.[34] The relationship between the potential curves for thermal and optical electron transfer processes is illustrated in Figure 1. For the activation energy ($\Delta G^{\ddagger}$) of the thermal electron-transfer process between degenerate $M^{III}-M^{II}$ and $M^{II}-M^{III}$ states in a mixed-valence complex, the function of the rate constant for thermal electron transfer can be represented as[6,38,39]

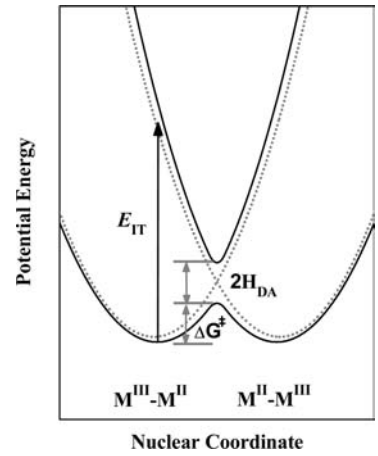

Figure 1. Potential energy curves for the diabatic limit (class I, dotted curve) and the weak coupling (class II, solid curve) in a mixed valence d^5-d^6 ion.

$$k_{et} = \kappa\upsilon_n e^{-\Delta G^{\ddagger}/RT} \quad (2)$$

where κ is the electronic transmission coefficient and υ_n is the nuclear frequency ($\upsilon_n \approx 5 \times 10^{12}$ s^{-1} at 298 K). For optical transfer, the E_{IT} energy of symmetric species can be expressed as[1,6]

$$E_{IT} = \lambda = \lambda_i + \lambda_o \quad (3)$$

$$\lambda_o = e^2\left(\frac{1}{2a_1} + \frac{1}{2a_2} - \frac{1}{r}\right)\left(\frac{1}{D_{OP}} - \frac{1}{D_S}\right) \quad (4)$$

where λ_i and λ_o are inner-sphere and solvent reorganization energies, e is the electronic charge transferred, a_1 and a_2 are radii of the spherical donor and acceptor, r is the separation between the donor and acceptor, and D_{OP} and D_S are the optical and static dielectric constants of the solvents.

According to several authors,[10,15,24,25,40] the comproportionation constant (K_c) for mixed-valence dimetal complexes is determined by the sum of five distinct factors that affect the magnitude of the free energy of comproportionation (ΔG_c) as follows:

$$-\Delta G_c = -(\Delta G_s + \Delta G_e + \Delta G_i + \Delta G_r + \Delta G_{ex}) \quad (5)$$

where ΔG_s, ΔG_e, ΔG_i, ΔG_r, and ΔG_{ex} are the statistical distribution of comproportionation equilibrium, the electrostatic repulsion between two metal centers, an inductive factor dealing with competitive coordination of the bridging ligand by the metal ions, the resonance contributions, and the electron exchange contributions, respectively. The $-\Delta G_e$ was evaluated using the method described by Elliott and Ferrere,[41] which assumes the calculated $-\Delta G_e$ between metal centers. For class II systems in a two-state model, the stability energy of the ground state ($-\varepsilon_s$) is determined by configu-

(18) Bixon, M.; Jortner, J. *Chem. Phys.* **2002**, *281*, 393.
(19) Mulliken, R. S.; Person, W. B. *Molecular Complexes*; Wiley-Intersicence: New York, 1967.
(20) Brunschwig, B. S.; Creutz, C.; Sutin, N. *Chem. Soc. Rev.* **2002**, *31*, 168.
(21) Shin, Y. K.; Brunschwig, B. S.; Creutz, C.; Newton, M. D.; Sutin, N. *J. Phy. Chem.* **1996**, *100*, 1104.
(22) Brunschwig, B. S.; Creutz, C.; Sutin, N. *Coord. Chem. Rev.* **1998**, *177*, 61.
(23) Robin, M. B.; Day, P. *Adv. Inorg. Chem. Radiochem.* **1967**, *10*, 247.
(24) Sutton, J. E.; Sutton, P. M.; Taube, H. *Inorg. Chem.* **1979**, *18*, 1017.
(25) Sutton, J. E.; Taube, H. *Inorg. Chem.* **1981**, *20*, 3125.
(26) Richardson, D. E.; Taube, H. *J. Am. Chem. Soc.* **1983**, *105*, 40.
(27) Ribou, A.-C.; Launay, J.-P.; Takahashi, K.; Nihira, T.; Tarutani, S.; Spangler, C. W. *Inorg. Chem.* **1994**, *33*, 1325.
(28) Patoux, G.; Coudret, C.; Launay, J.-P.; Joachim, C.; Gourdon, A. *Inorg. Chem.* **1997**, *36*, 5037.
(29) Ribou, A.-C.; Launay, J.-P.; Sachtleben, M. L.; Li, H.; Spangler, C. W. *Inorg. Chem.* **1996**, *35*, 3735.
(30) Zhu, Y.; Clot, O.; Wolf, M. O.; Yap, G. P. A. *J. Am. Chem. Soc.* **1998**, *120*, 1812.
(31) Xu, G.-L.; Crutchley, R. J.; DeRosa, M. C.; Pan, Q.-J.; Zhang, H.-X.; Wang, X.; Ren, T. *J. Am. Chem. Soc.* **2005**, *127*, 13354.
(32) Curtis, J. C.; Sullivan, B. P.; Meyer, T. J. *Inorg. Chem.* **1983**, *22*, 224.
(33) Chang, J. P.; Fung, E. Y.; Curtis, J. C. *Inorg. Chem.* **1986**, *25*, 4233.
(34) Neyhart, G. A.; Hupp, J. T.; Curtis, J. C.; Timpson, C. J.; Meyer, T. J. *J. Am. Chem. Soc.* **1996**, *118*, 3724.
(35) Liu, T.-Y.; Chen, Y. J.; Tai, C.-J.; Kwan, K. S. *Inorg. Chem.* **1999**, *38*, 674.
(36) Chen, Y. J.; Kao, C.-C.; Lin, S. J.; Tai, C.-J.; Kwan, K. S. *Inorg. Chem.* **2000**, *39*, 189.
(37) Gutmann, V. *The Donor-Acceptor Approach to Molecular Interactions*; Plenum: New York, 1978.
(38) Sutin, N. *Acc. Chem. Res.* **1982**, *15*, 275.
(39) Sutin, N. *Prog. Inorg. Chem.* **1983**, *30*, 441.
(40) Evans, C. E. B.; Naklicki, M. L.; Rezvani, A. R.; White, C. A.; Kondratiev, V. V.; Crutchley, R. J. *J. Am. Chem. Soc.* **1998**, *120*, 13096.
(41) Ferrere, S.; Elliott, C. M. *Inorg. Chem.* **1995**, *34*, 5818.

rational mixing between the donor and acceptor, as represented by the following equation:[10]

$$-\varepsilon_s = \frac{H_{DA}^2}{E_{IT}} \quad (6)$$

For weak coupling systems, $-\Delta G_r$ is defined by eq 7.[10,40]

$$-\Delta G_r = -2\varepsilon_s \quad (7)$$

The electron-exchange contributions to the free energy of comproportionation, $-\Delta G_{ex}$, can be expressed by the antiferromagnetic exchange term (J_{af}) in a two-electron system, as described by Bertrand[42] and Tuczek and Solomon.[43] Three-state models of these systems are more complicated and involve efficient coupling of the donor and acceptor with the BL. The important features of the optical electron-transfer among the D−BL−A system in complexes of three-state models include the following: (a) coupling elements between the relevant orbitals of the BL and the relational orbitals in terminals D and A that are capable of mediating D/A coupling[7,13,20,40,44] and (b) the effect of efficient coupling on the energy of the D/A charge-transfer absorption.[7,8,10,14−17,45] Furthermore, D/A coupling is related to the bridging state by linker-mediated vibronic effects.[46] The observed properties of intervalence transfer between the terminal metal and bridging moiety of multimetal complexes can alter the superexchange couplings calculated using the model of Creutz, Newton, and Sutin (CNS model).[7,8,13,40,47−50] When the direct coupling of the donor and acceptor is neglected ($H_{DA} \approx 0$), E_{ML} (metal-to-ligand energy) > E_{IT} and the CNS model for evaluating superexchange D/A coupling mediating by the bridging ligand, H_{DA}^S,[7,8] of mixed-valence dimetal complexes includes strong coupling between the terminal $d\pi$ orbitals and the orbitals of the bridging ligand as follows:[7,8,51]

$$H_{DA}^S = \frac{H_{ML}H_{M'L}}{2\Delta E_{ML}^{eff}} + \frac{H_{LM}H_{LM'}}{\Delta E_{LM}^{eff}} \quad (8)$$

where H_{ML}($H_{M'L}$) and H_{LM}($H_{LM'}$) are the coupling elements between the orbitals of the terminal metal-center and the relational bridging orbital. ΔE_{ML}^{eff} and ΔE_{LM}^{eff} are the effective energy gaps for optical electron transfer, and ΔE_{ML}^{eff} is given by the equation $\Delta E_{ML}^{eff} = \{0.5 \times [1/E_{ML} + 1/(E_{ML} - E_{IT})]\}^{-1}$. Here, E_{ML} and E_{IT} are the vertical excitation energies for the metal-to-ligand and intervalence transfer between D and A, respectively. With some perturbation theory corrections,

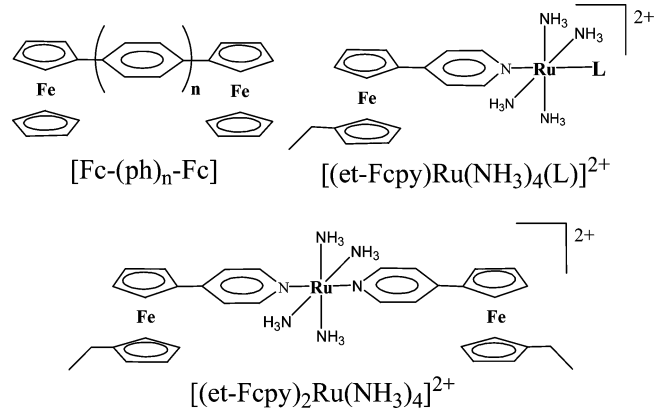

Figure 2. The symbols of selected *trans*-dimetal complexes, [Fc−(ph)$_n$−Fc] and [(et-Fcpy)Ru(NH$_3$)$_4$(L)]$^{2+}$, for $n = 0$, [Fc−Fc]; $n = 1$, [Fc−(ph)−Fc]; $n = 2$, [Fc−(ph)$_2$−Fc] and L = NH$_3$, [(et-Fcpy)Ru(NH$_3$)$_5$]$^{2+}$; pyridine, [(et-Fcpy)Ru(NH$_3$)$_4$(py)]$^{2+}$; and the trans-trimetal complex, [(et-Fcpy)$_2$Ru(NH$_3$)$_4$]$^{2+}$.

covalently linked di- and trimetal complexes can also be described by the CNS model.[13,40,47−49]

In this article, we provide detailed evidence that the highly efficient coupling between a state containing the central ruthenium(m)ine and a state including the terminal $Fe^{II}-Fe^{III}$/$Fe^{III}-Fe^{II}$ combination mediates the significant end-to-end interaction in an unusual three-state condition. We synthesized bridging biferrocene complexes, a heterobimetallic complex of ferrocenyl−rutheniumam(m)ine−pyridinyl ions, and a symmetric trimetal complex of ferrocenyl−rutheniumam(m)ine−ferrocenyl, as shown in Figure 2.

Experimental Section

1. Materials and Synthesis of Compounds. Ferrocene (Fc), pyridine (py), and 4-bromopyridine hydrochloride were purchased from Aldrich, and [Ru(NH$_3$)$_6$]Cl$_3$ and NH$_4$PF$_6$ were purchased from STREM. The syntheses of [Ru(NH$_3$)$_5$Cl]Cl$_2$, *trans*-[Ru(NH$_3$)$_4$Cl$_2$]Cl, *trans*-[Ru(NH$_3$)$_4$(py)(H$_2$O)](PF$_6$)$_2$, and *trans*-[Ru(NH$_3$)$_4$(H$_2$O)$_2$](PF$_6$)$_2$ have been reported previously.[33,52] The 1-ethyl-1′-(4-pyridyl)ferrocene (et-Fcpy) and [(et-Fcpy)Ru(NH$_3$)$_5$](PF$_6$)$_2$ were prepared as described previously.[36] Bromoferrocene, biferrocene ([Fc−Fc]), *p*-phenylbiferrocene ([Fc−(ph)−Fc]), and 4,4′-bromoferrocenylbiphenyl ([Fc−(ph)$_2$−Br]) were synthesized according to procedures in the literature.[28,53−55]

***trans*-[(et-Fcpy)Ru(NH$_3$)$_4$(py)](PF$_6$)$_2$.** A sample of 200 mg of *trans*-[Ru(NH$_3$)$_4$(py)(H$_2$O)](PF$_6$)$_2$ (0.36 mmol) and a sample of 110 mg of 1-ethyl-1′-(4-pyridyl)ferrocene (0.38 mmol) were added to 10 mL of a degassed acetone solution under argon, and the mixture was stirred for 2 h. Then, 100 mL of degassed ether was slowly added to the reaction flask in an ice bath, and the resulting orange product was removed by filtration. The fresh product was dissolved in 5 mL of acetone and then was mixed with 10 mL of water containing 5 g of NH$_4$PF$_6$, followed by cooling in an ice bath. The volume of the solution was reduced to 10 mL in the ice bath, and the orange precipitate was then removed by filtration. The product was washed with 1 mL of cold water followed by a second wash with 10 mL of cold ether. The product was dried in an oven under

(42) Bertrand, P. *Chem. Phys. Lett.* **1985**, *113*, 104.
(43) Tuczek, F.; Solomon, E. I. *Inorg. Chem.* **1993**, *32*, 2850.
(44) Zusman, L. D.; Beratan, J. *Chem. Phys.* **1999**, *110*, 10468.
(45) Salaymeh, F.; Berhane, S.; Yusof, R.; Rosa, R.; Fung, E. Y.; Matamoros, R.; Lau, K. W.; Zheng, Q.; Kober, E. M.; Curtis, J. C. *Inorg. Chem.* **1993**, *32*, 3895.
(46) McConnell, H. M. *J. Chem. Phys.* **1961**, *35*, 508.
(47) Watzky, M. A.; Macatangay, A. V.; Van Camp, R. A.; Song, X.; Endicott, J. F.; Buranda, T. *J. Phys. Chem. A* **1997**, *101*, 8441.
(48) Macatangay, A. V.; Mazzetto, S. E.; Endicott, J. F. *Inorg. Chem.* **1999**, *38*, 5091.
(49) Macatangay, A.; Endicott, J. F. *Inorg. Chem.* **2000**, *39*, 437.
(50) Browne, W. R.; Hage, R.; Vos, J. G. *Coord. Chem. Rev.* **2006**, *250*, 1683.
(51) Newton, M. D. In *Electron Transfer in Chemistry*; Balzani, V., Ed.; Wiley-VCH: Weinheim, Germany, 2001; Vol. 1, p 3.
(52) Krentzien, H. J. Ph.D. paper, Stanford University, Palo Alto, CA, 1976.
(53) Fish, R. W.; Rosenblum, M. *J. Org. Chem.* **1965**, *30*, 1253.
(54) Beletskaya, I. P.; Tsvetkov, A. V.; Latyshev, G. V.; Tafeenko, V. A.; Lukashev, N. V. *J. Organomet. Chem.* **2001**, *637−639*, 653.
(55) Brown, G. M.; Meyer, T. J.; Cowan, D. O.; Levanda, C.; Kanfman, F.; Roling, P. V.; Rausch, M. D. *Inorg. Chem.* **1975**, *14*, 506.

a vacuum. The fresh product yield was approximately 40%. For *trans*-[(et-Fcpy)Ru(NH_3)$_4$(py)](PF_6)$_2$, anal. calcd for $C_{22}H_{34}F_{12}FeN_6P_2Ru$: C, 31.86; H, 4.13; N, 10.13. Found: C, 31.99; H, 3.99; N, 9.98. ^{1}H NMR (acetone-d_6): δ 1.07(t, 3H), 2.23(q, 2H), 2.72(s, 12H), 3.93(t, 2H), 3.98(t, 2H), 4.50(t, 2H), 4.93(t, 2H), 7.48(t, 2H), 7.58(d, 2H), 7.88(t, 1H), 8.62(d, 2H), 8.80(d, 2H).

***trans*-[(et-Fcpy)$_2$Ru(NH_3)$_4$](PF_6)$_2$.** A total of 20 mL of degassed acetone solution containing *trans*-[Ru(NH_3)$_4$(H_2O)$_2$](PF_6)$_2$ (80 mg, 0.16 mmole) and 1-ethyl-1′-(4-pyridyl)ferrocene (94 mg, 0.32 mol) was stirred for 2 h under argon. Afterward, 100 mL of degassed ether was added to the acetone solution, and the mixture was kept at 0 °C for 10 min. The resulting orange precipitate was removed by filtration and then was washed with ether. The fresh product was dissolved in 5 mL of acetone, and then 100 mL of ether was added to the acetone solution. The mixture was cooled to 0 °C for 10 min, and the orange precipitate was removed by filtration. The fresh product yield was approximately 30%. For *trans*-[(et-Fcpy)$_2$Ru(NH_3)$_4$](PF_6)$_2$, anal. calcd for $C_{34}H_{46}F_{12}Fe_2N_6P_2Ru$: C, 39.21; H, 4.45; N, 8.07. Found: C, 39.52; H, 4.72; N, 7.95. ^{1}H NMR (acetone-d_6): δ 1.09(t, 6H), 2.22(q, 4H), 2.80(s, 12H), 3.95(t, 4H), 4.04(t, 4H), 4.50(t, 4H), 4.94(t, 4H), 7.60(d, 4H), 8.64(d, 4H).

***p*-Biphenylbiferrocene, [Fc−(ph)$_2$−Fc].** A 1 g sample of magnesium was added to a round bottle containing 50 mL of dry THF (tetrahydrofuran) under N_2, and then 0.1 mL of 1,2-dibromoethane was added to the THF solution. After 10 min, the THF solution was combined with 20 mL of a THF solution containing 1.06 g of bromoferrocene (4 mmol) and stirred for 2 h under N_2. The orange solution was transferred to a round bottle containing a sample of 0.834 g of 4,4′-ferrocenylbromobiphenyl (2 mmol) and 50 mg of 1,3-bis(diphenylphosphino)-propane nickel(II) chloride. The reaction solution was refluxed for 2 days under N_2 and then was cooled to room temperature. The reaction was quenched with 50 mL of methanol, and the solution was concentrated and chromatographed (Al_2O_3) with CH_2Cl_2 to yield 150 mg (15%) of the product. For *p*-biphenylbiferrocene ([Fc−(ph)$_2$−Fc]), anal. calcd for $C_{32}H_{26}Fe_2$: C, 73.60; H, 5.02. Found: C, 73.25; H, 5.12. ^{1}H NMR($CDCl_3$): δ 4.10(s, 10H), 4.38(t, 4H), 4.72(t, 4H), 7.54(s, 8H).

2. Instrumentation. Electrochemical measurements were performed using an Epsilon electrochemical workstation. Cyclic voltammograms (CV) and differential pulse voltammograms (DPV) were obtained in dry CH_3CN, DMSO, DMF, DMA, 2-butanone, propandiol-(1,2)-carbonate (PC), benzonitrile, propionitrile, nitromethane, acetone, and nitrobenzene using a three-electrode system consisting of a Ag/AgCl reference electrode, a Pt-wire counter electrode, and a Pt-disk working electrode. The complex was dissolved in various solvents containing 0.1 M tetrabutylammonium hexafluorophosphate (TBAH) as the electrolyte. Ferrocene was the internal reference (0.437 V vs Ag/AgCl in CH_3CN) for the CV. UV−visible−NIR spectra were recorded using a Shimadzu UV-3101PC spectrophotometer. For measurement of the intervalence charge-transfer spectra, 5 mL of either the di- or trimetal complex solution (2×10^{-3} M) was mixed with 5 mL of either a 2×10^{-3} M ferrocenium or 10^{-3} M iodine solution in the same solvent. An aliquot of the mixture was transferred to a 1 cm quartz cell.

3. X-Ray Crystallography. Single crystals were obtained by the slow diffusion of ether into a saturated chloroform solution containing [Fc−(ph)$_2$−Fc]. Diffraction data were measured using a Bruker P4 diffractometer with Mo radiation. Cell parameters were determined from 25 accurately centered reflections in the range $0° \leq 2\theta \leq 30°$. Three standard reflections were monitored every 100 reflections during data collection, and no variation was observed. The crystal structure of [Fc−(ph)$_2$−Fc] was solved and refined using Bruker SHELXTL PC software. A summary for the crystallographic parameters of [Fc−(ph)$_2$−Fc] is presented in Table S1, and additional details are provided in the Supporting Information (Tables S2−S4). An ORTEP drawing of [Fc−(ph)$_2$−Fc] is shown in Figure S1 (Supporting Information).

4. Computational Methods. The quantum mechanical calculations reported in this paper were performed using the density functional theory method with the Becke three-parameter hybrid functional B3LYP.[56] Dunning−Huzinaga valence double-ξ basis sets[57] were used for hydrogen, carbon, and nitrogen; iron and ruthenium were described by the effective core potential plus double-ξ basis set developed by Hay and Wadt.[58] Restricted and unrestricted calculations were adopted to characterize the closed-shell electronic structure of [(et-Fcpy)$_2$Ru(NH_3)$_4$]$^{4+}$ and the open-shell electronic structure of [Fc−(ph)$_2$−Fc]$^+$, respectively. The geometries of [(et-Fcpy)$_2$Ru(NH_3)$_4$]$^{4+}$ and [Fc−(ph)$_2$−Fc]$^+$ were optimized under the C_{2h} symmetry constraint, which is a reasonable approximation of the transition state structure during charge transfer. All of the calculations were performed using the Gaussian 03 program.[59]

Results

1. Electrochemistry. The basic electrochemical data for the di- and trimetal complexes in various solvents are summarized in Table 1. Results of the demonstrative DPV studies of [(et-Fcpy)Ru(NH_3)$_4$(py)]$^{2+}$ and of [(et-Fcpy)$_2$Ru(NH_3)$_4$]$^{2+}$ in DMSO, acetone, acetonitrile, and nitromethane are shown in Figure 3. The $E_{1/2}(Ru^{III/II})$ of [(et-Fcpy)Ru(NH_3)$_4$(py)]$^{2+}$ and [(et-Fcpy)$_2$Ru(NH_3)$_4$]$^{2+}$ ranged between −0.30 and +0.40 V in the various solvents tested, consistent with the $E_{1/2}(Ru^{III/II})$ behaviors of the rutheniumam(m)ine moiety, as reported in the early literature.[32−34,36,60,61] For [(et-Fcpy)Ru(NH_3)$_5$]$^{2+}$ in various solvents, the relatively small $E_{1/2}(Ru^{III/II})$ was in contrast to the $E_{1/2}(Fe^{III/II})$ of the ferrocenyl moiety.[36] The electrochemical behaviors of [(et-Fcpy)Ru(NH_3)$_4$(py)]$^{2+}$ and [(et-Fcpy)$_2$Ru(NH_3)$_4$]$^{2+}$ in various solvents were similar (range of DN between 29.8 (DMSO) and 11.9 (benzonitrile)), $E_{1/2}(Fe^{III/II}) > E_{1/2}(Ru^{III/II})$; however, in both nitrobenzene and nitromethane, $E_{1/2}(Ru^{III/II}) > E_{1/2}(Fe^{III/II})$. For the DPV studies of [(et-Fcpy)$_2$Ru(NH_3)$_4$]$^{2+}$ in Figure 3, an $E_{1/2}(Fe^{III/II})$ peak due to two ferrocenyl moieties was observed in DMSO, acetone, and nitromethane, and a couple of $E_{1/2}(Fe^{III/II})$ peaks associated with the two ferrocenyl moieties were observed in acetonitrile. We observed similar behaviors in two other nitriles, propionitrile and benzonitrile. The $\Delta E_{1/2(2)}$ ($E_{1/2(2)}(Fe^{III/II}) - E_{1/2(1)}(Fe^{III/II})$) values for [(et-Fcpy)$_2$Ru($NH_3$)$_4$]$^{2+}$ in propionitrile, acetonitrile, and benzonitrile were 83, 99, and 108 mV, respectively. In nitromethane and nitrobenzene, the single $E_{1/2}(Fe^{III/II})$ peak of the two ferrocenyl moieties was relatively less than the $E_{1/2}(Ru^{III/II})$.

(56) Becke, A. D. *J. Chem. Phys.* **1993**, *98*, 5648.
(57) Dunning, T. H., Jr.; Hay, P. J.; Schaefer, H. F. Plenum: New York, 1976; p 1−28.
(58) Hay, P. J.; Wadt, W. R. *J. Chem. Phys.* **1985**, *82*, 299.
(59) Frisch, M. J. *Gaussian 03*, revision D.02 ed.; Gaussian Inc.: Pittsburgh, PA, 2003.
(60) Matsubara, T.; Ford, P. C. *Inorg. Chem.* **1976**, *5*, 1107.
(61) Creutz, C.; Chou, M. H. *Inorg. Chem.* **1987**, *26*, 2995.

Table 1. Half-Wave Potentials vs $E_{1/2}$ ($Fc^{+1/0}$) of the Complexes[a]

		[(et-Fcpy)Ru(NH$_3$)$_5$]$^{2+}$[b]			[(et-Fcpy)Ru(NH$_3$)$_4$ (py)]$^{2+}$[c,d]			[(et-Fcpy)$_2$Ru(NH$_3$)$_4$]$^{2+}$[c,d]			
solvents	D.N.	$E_{1/2}(Ru^{III/II})$	$E_{1/2}(Fe^{III/II})$	$\Delta E_{1/2(1)}$	$E_{1/2}(Ru^{III/II})$	$E_{1/2}(Fe^{III/II})$	$\Delta E_{1/2(1)}$	$E_{1/2}(Ru^{III/II})$	$E_{1/2}(Fe^{III/II})$	$\Delta E_{1/2(1)}$	$\Delta E_{1/2(2)}$[e]
DMSO	29.8	−510	130	640	−267	154	421	−305	160	465	≤70
DMA	27.8	−498	142	640	−248	195	443	−313	149	462	≤70
DMF	26.6	−462	141	603	−206	171	377	−279	159	438	≤70
2-butanone	20				−22	145	167	−92	159	251	≤70
CH_3OH	19	−229	133	362							
Acetone	17	−250	131	381	−12	166	178	−72	163	235	≤70
propionitrile	16.1				63	199	136	−18	127, 210	145[f]	83
PC[g]	15.1	−187	156	343	42	202	160	−8	189	197	≤70
acetonitrile	14.1	−118	179	297	71	213	142	30	156, 255	126[f]	99
benzonitrile	11.9	−153	137	290	34	181	147	−15	101, 209	116[f]	108
nitrobenzene	4.4	−34	136	170	287	73	214	300	66	234	≤70
nitromethane	2.7	43	173	130	339	95	244	398	98	300	≤70

[a] Potentials in millivolts; electrolyte/solvent, 0.1 M TBAH/solvent; Ag/AgCl reference electrode; $E_{1/2}$ of ferrocene in CH_3CN is 0.437 V; $\Delta E_{1/2(1)} = E_{1/2}(Fe^{III/II}) - E_{1/2}(Ru^{III/II})$. [b] Cyclic voltammetry; sweep rate, 100 mV/s. [c] This work. [d] Differential pulse voltammetry, sweep rate, 4 mV/s. [e] $\Delta E_{1/2(2)} = E_{1/2(second)}(Fe^{III/II}) - E_{1/2(first)}(Fe^{III/II})$. [f] $\Delta E_{1/2(1)} = E_{1/2(first)}(Fe^{III/II}) - E_{1/2}(Ru^{III/II})$. [g] Propandiol-(1,2)-carbonate.

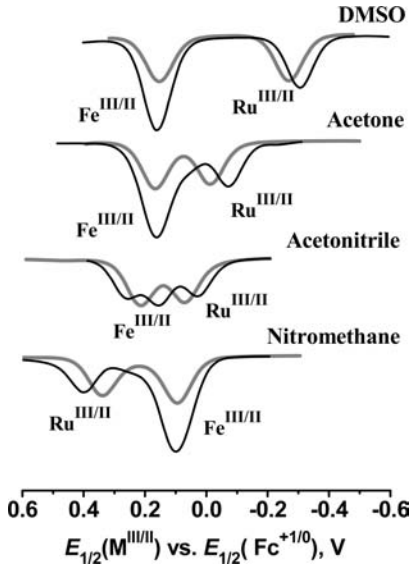

Figure 3. The differential pulse voltammograms (DPV) of [(et-Fcpy)Ru(NH$_3$)$_4$(py)]$^{2+}$, gray curves, and [(et-Fcpy)$_2$Ru(NH$_3$)$_4$]$^{2+}$, black curves.

Among biferrocene systems with linked polyphenyl moieties, specifically among the [Fc−(ph)$_n$−Fc] series, where $n = 0-2$, $E_{1/2}(Fe^{III/II})$ peaks were observed in nitrobenzene. The $\Delta E_{1/2}(Fe^{III/II}-Fe^{III/II})$ peaks of [Fc−Fc] and [Fc−(ph)−Fc] were observed at 350 and 101 mV, respectively, and [Fc−(ph)$_2$−Fc] had a broad $E_{1/2}(Fe^{III/II})$ peak. According to unpublished results,[62] the $\Delta E_{1/2}(Fe^{III/II}/Fe^{III/II})$ of 4-(1-ethylferrocenyl)-4′-ferrocenylbiphenyl ([et-Fc−(ph)$_2$−Fc]) is 70 mV, and therefore, we assumed that the $\Delta E_{1/2}(Fe^{III/II}/Fe^{III/II})$ of [Fc−(ph)$_2$−Fc] ranged between 36 and 70 mV (K_c between 4 and 15). Results of the electrochemical studies of [Fc−(ph)$_n$−Fc] are summarized in Table 2, and the original studies of [Fc−Fc] and [Fc−(ph)−Fc] were reported previously.[28,63]

2. UV−Vis Absorption Spectra. The absorption spectra of et-Fcpy and [(et-Fcpy)Ru(NH$_3$)$_5$]$^{2+/3+}$ in acetonitrile were described in our previous report,[36] while the absorption properties of [(et-Fcpy)Ru(NH$_3$)$_4$(py)]$^{2+/3+}$ and [(et-Fcpy)$_2$Ru(NH$_3$)$_4$]$^{2+/3+}$ are summarized in Table 3. The demonstrative absorption spectra of [(et-Fcpy)Ru(NH$_3$)$_4$-(py)]$^{2+/3+}$ in DMSO and nitromethane are shown in Figure S2 (Supporting Information). The very intense maxima of metal-to-ligand charge-transfer (MLCT) absorption for the Ru^{II}−py moieties of [(et-Fcpy)Ru(NH$_3$)$_4$(py)]$^{2+}$ and [(et-Fcpy)$_2$Ru(NH$_3$)$_4$]$^{2+}$ ranged between 400 and 550 nm in DMSO and nitromethane. The relatively weak absorption at 467 nm (465 nm) in DMSO for [(et-Fcpy)Ru(NH$_3$)$_4$(py)]$^{3+}$ ([(et-Fcpy)$_2$Ru(NH$_3$)$_4$]$^{3+}$) was assigned to weak d−d absorption of the ferrocenyl moiety. Furthermore, under nitromethane conditions, the intense absorption bands at 420 and 498 nm (441 and 491 nm) were assigned to MLCT absorption of the Ru^{II}−py and Ru^{II}−py−Fc^+ moieties for [(et-Fcpy)Ru(NH$_3$)$_4$(py)]$^{3+}$ (Ru^{II}−py−Fc and Ru^{II}−py−Fc^+ moieties for [(et-Fcpy)$_2$Ru(NH$_3$)$_4$]$^{3+}$); in addition, the weak absorption (shoulder, ≈600 nm) was assigned to d−d absorption of the ferrocenium moiety for both complexes. This assignment is consistent with the spectra of ferrocene, which have been extensively studied.[64,65]

3. Intervalence Charge-Transfer Properties. The absorption energies (E_{IT}), absorbance maximum (ε_{max}), and the half-width ($\Delta\nu_{1/2}$) for the pertinent intervalence transfer (IT) properties of the mixed-valence [Fc−(ph)$_n$−Fc]$^+$ series, $n = 0-2$, are summarized in Table 2, and the IT spectra are shown in Figure 4. The reorganization energies ($\lambda = E_{IT}$) of [Fc−(ph)$_n$−Fc]$^+$ were 5200, 7300, and 9000 ± 500 cm^{-1} for $n = 0$, 1, and 2, respectively. The two-state model shown in Figure 1 simply illustrates the basic properties of the [Fc−(ph)$_n$−Fc]$^+$ series.

Because the IT spectral bandwidth of the mixed-valence complexes, such as [(et-Fcpy)Ru(NH$_3$)$_5$]$^{3+}$, [(et-Fcpy)Ru(NH$_3$)$_4$(py)]$^{3+}$, and [(et-Fcpy)$_2$Ru(NH$_3$)$_4$]$^{3+}$, is broad (between 3600 and 4300 cm^{-1}) and unstructured, it was fit to a Gaussian function using OriginPro 7.0, as shown in Table 4. Typically, the intervalence energies of [(et-Fcpy)Ru(NH$_3$)$_5$]$^{3+}$ in various solvents are transferred from the Fe^{II}−Ru^{III} state to the Fe^{III}−Ru^{II} state. Moreover, the increased IT energies are influenced by various solvents, ranging from DMSO to nitromethane, depending on the

(62) Chen, W.-T. Unpublished results, Fu Jen Catholic University, Taiwan, 2003.
(63) Brown, G. M.; Meyer, T. J.; Cowan, D. O.; LeVanda, C.; Kaufman, F.; Roling, P. V.; Rausch, M. D. *Inorg. Chem.* **1965**, *14*, 506.
(64) Scott, D. R.; Becker, R. S. *J. Chem. Phys.* **1962**, *35*, 516.
(65) Scott, D. R.; Becker, R. S. *J. Chem. Phys.* **1962**, *35*, 2246.

Table 2. Electrochemical and Intervalence Spectral Properties of [Fc−(ph)$_n$−Fc] Series

complexes	$E_{1/2}$ vs $E_{1/2}(Fc^{+1/0})$[a]	$\Delta E_{1/2}$[b]	K_c[c]	r_{MM} (Å)[d]	E_{IT}, cm^{-1}/10,[3e] (ε_{max}/10^3),[f] [$\Delta\upsilon_{1/2}$/10^3][g]	H_{DA} (cm^{-1})[h]
[Fc−Fc]	−87, 263	350	8.40×10^5	5.1[i]	5.2 ± 0.1, (1.0), [3.9 ± 0.1]	560
[Fc−(ph)−Fc]	−12, 89	101	51	8.8[j]	7.3 ± 0.1, (0.70), [3.9 ± 0.1]	330
[Fc−(ph)$_2$−Fc]	30	<70	>4, <15	13.0[k]	9.0 ± 0.5, (0.23),[3.6 ± 1.0]	140

[a] Cyclic voltammetry in nitrobenzene containing 0.1 M TBAH, scan rate = 100 mV/s. $E_{1/2}$ of ferrocene ($E_{1/2}(Fc^{+1/0})$) is the new origin. [b] $\Delta E_{1/2} = E_{1/2(2)} - E_{1/2(1)}$. [c] Comproportionation constant. [d] Metal-to-metal distance. [e] Intervalence charge-transfer absorption of [Fc−(ph)$_n$−Fc]$^+$. [f] Extinction coefficient. [g] Half-intensity width. [h] Equation 1. [i] Reference 67. [j] Reference 28. [k] This work.

Table 3. Absorption Spectra of [(et-Fcpy)Ru(NH$_3$)$_4$(py)]$^{n+}$ and [(et-Fcpy)$_2$Ru(NH$_3$)$_4$]$^{n+}$ (n = 2, 3) in DMSO and Nitromethane

	DMSO		nitromethane	
complexes	λ_{max} (nm)[a]	[ε_{max} (M^{-1} cm^{-1})/ 10^3][b]	λ_{max} (nm)[a]	[ε_{max} (M^{-1}cm^{-1})/ 10^3][b]
[(et-Fcpy)Ru (NH$_3$)$_4$(py)]$^{2+}$[c]	284	[8.9]	430	[19.0]
	375(sh)	[3.6]		
	472	[19.0]		
[(et-Fcpy)Ru (NH$_3$)$_4$(py)]$^{3+}$[c]	301(sh)	[27.0]	420	[9.6]
	379(sh)	[6.6]	498	[7.9]
	467	[3.0]	600(sh)	[4.4]
	1019	[0.64]	1281	[0.62]
[(et-Fcpy)$_2$Ru (NH$_3$)$_4$]$^{2+}$	284	[18.6]	452	[23.3]
	381(sh)	[4.1]		
	526	[27.6]		
[(et-Fcpy)$_2$Ru (NH$_3$)$_4$]$^{3+}$	324(sh)	[19.3]	441	[12.5]
	381(sh)	[11.0]	491	[12.4]
	465	[5.0]	600(sh)	[6.8]
	1036	[1.1]	1360	[0.86]

[a] Absorption maximia. [b] Extinction coefficient. [c] Figure S2, Supporting Information.

solvent donicity.[35,36] The IT energies of the [(R-Fcpy)Ru(NH$_3$)$_5$]$^{3+}$ series in nitrobenzene and nitromethane were less than the IT energies of the [(R-Fcpy)Ru(NH$_3$)$_5$]$^{3+}$ series in acetonitrile by approximately 1800−2300 cm^{-1} (R = ethyl, H, Br, and acetyl).[35,36] For [(et-Fcpy)Ru(NH$_3$)$_4$-(py)]$^{3+}$, the IT energy versus the solvent donicity (D.N.) relationship decreased in various solvents, ranging from DMSO to benzonitrile. However, the IT energies in nitrobenzene and nitromethane were more similar to the IT energies in acetonitrile. The intervalence absorptions of [(et-Fcpy)Ru(NH$_3$)$_5$]$^{3+}$ and [(et-Fcpy)Ru(NH$_3$)$_4$(py)]$^{3+}$ in DMSO, acetone, acetonitrile, nitrobenzene, and nitromethane are shown in Figure S3 (Supporting Information). In Figure S4 (Supporting Information), the slopes of the least-squares lines for E_{IT} versus D.N. were 22 ± 1, 23 ± 2, and 21 ± 1 meV/D.N. for [(et-Fcpy)Ru(NH$_3$)$_5$]$^{3+}$, [(et-Fcpy)Ru(NH$_3$)$_4$(py)]$^{3+}$, and [(et-Fc)$_2$Ru(NH$_3$)$_4$]$^{3+}$ in various solvents, respectively. The E_{IT} of [(et-Fcpy)Ru(NH$_3$)$_4$(py)]$^{3+}$ and [(et-Fc)$_2$Ru-(NH$_3$)$_4$]$^{3+}$ in nitrobenzene and nitromethane deviated from the least-squares lines. The intervalence transfer behavior of [(et-Fc)$_2$Ru(NH$_3$)$_4$]$^{3+}$ in various solvents was similar to the behaviors of [(et-Fcpy)Ru(NH$_3$)$_4$(py)]$^{3+}$. The influence of the solvent donicity on E_{IT} energies of [(et-Fcpy)Ru(NH$_3$)$_5$]$^{3+}$, [(et-Fcpy)Ru(NH$_3$)$_4$(py)]$^{3+}$, and [(et-Fc)$_2$Ru(NH$_3$)$_4$]$^{3+}$ in various solvents was clearly evident in a similar optical intervalence transfer from the Fe^{II}−Ru^{III} state to the Fe^{III}−Ru^{II} state.[35,36] However, the intervalence transfer of [(et-Fcpy)Ru(NH$_3$)$_4$(py)]$^{3+}$ and [(et-Fc)$_2$Ru(NH$_3$)$_4$]$^{3+}$ in nitrobenzene and nitromethane corresponds to a transition from the Fe^{III}−Ru^{II} state to the Fe^{II}−Ru^{III} state. The relationships between the Fe^{II}−Ru^{III} and Fe^{III}−Ru^{II} states for [(et-Fcpy)Ru(NH$_3$)$_4$(py)]$^{3+}$ and [(et-Fc)$_2$Ru(NH$_3$)$_4$]$^{3+}$ cations in various solvents are shown qualitatively by the PE plot in Figure S5 (Supporting Information). Intervalence-transfer absorption of the [(et-Fc)$_2$Ru(NH$_3$)$_4$]$^{4+}$ cation was not observed when the dark precipitate was exposed to 2 equiv. of the oxidizing reagent and mixed with 1 equiv of the [(et-Fcpy)$_2$Ru(NH$_3$)$_4$]$^{2+}$ ion.

Discussion

1. Diferrocenyl Cation. The series of mixed valence [Fc−(ph)$_n$−Fc]$^+$ cations, n = 0−2, exhibited increasing intervalence energies with increasing bridging-chain lengths (metal-to-metal distance, r = 5.1,[66,67] 8.8,[28] and 13.0 Å for n = 0, 1, and 2, respectively). The H_{DA} values between the donor and acceptor states of [Fc−(ph)$_n$−Fc]$^+$ calculated using eq 1 were 560 cm^{-1} for n = 0, 330 cm^{-1} for n = 1, and 140 ± 50 cm^{-1} for n = 2 (see Table 2). Qualitatively, according to eq 4, the reorganizational energy tends to increase with increasing separation between the donor and acceptor, but according to eq 1, H_{DA} should decrease. The upper limit of the sum of $\Delta G^{\ddagger}$ and H_{DA} for the outer-sphere self-exchange of the Fc$^+$/Fc^0 couple in solutions is approximately 2500 cm^{-1};[68,69] thus, the reorganization energy for Fc$^+$/Fc^0 self-exchange is approximately 10000 cm^{-1}. In addition, the 1300 cm^{-1} of reorganization energy for Fc$^+$/Fc^0 self-exchange in the gas phase[68] indicates a solvent reorganizational energy in the range of 8700 cm^{-1} for Fc$^+$/Fc^0 self-exchange in solution. The vertical E_{IT} of the diabatic limit for the system of [Fc−BL−Fc]$^+$ should be greater than 10000 cm^{-1}. Thus, the relatively large E_{IT} of [Fc−(ph)$_2$−Fc]$^+$ in nitrobenzene approached the diabatic limit. For the weakly coupled [Fc−(ph)$_n$−Fc]$^+$ cation, the activation energy ($\Delta G^{\ddagger}$) between the donor and acceptor is typically calculated as follows:[1,6]

$$\Delta G^{\ddagger} = \frac{E_{IT}}{4} - H_{DA} \qquad (9)$$

where the matrix element can be evaluated using eq 1. The calculated values of $\Delta G^{\ddagger}$ for n = 0, 1, and 2 were 690, 1500, and 2100 cm^{-1}, respectively. The basic results of electrochemistry and intervalence absorption for the series of [Fc−(ph)$_n$−Fc]$^+$ cations in this study are summarized in Table 2. The basis of intervalence transfer and electrochemistry for [Fc−Fc]$^+$ and [Fc−ph−Fc]$^+$ was reported in the early literature.[28,55,67] The stability energies ($-\varepsilon_s$) calculated using eq 6 for the ground state of the [Fc−(ph)$_n$−Fc]$^+$ series

(66) Macdonald, A. C.; Trotter, J. *Acta Crystallogr.* **1964**, *17*, 872.
(67) Crown, D. O.; Kaufman, F. *J. Am. Chem. Soc.* **1970**, *92*, 219.
(68) Phelps, D. K.; Gord, J. R.; Freiser, B. S.; Weaver, M. J. *J. Phys. Chem.* **1991**, *95*, 4338.
(69) Weaver, M. J.; McManis, G. E. *Acc. Chem. Res.* **1990**, *23*, 294.

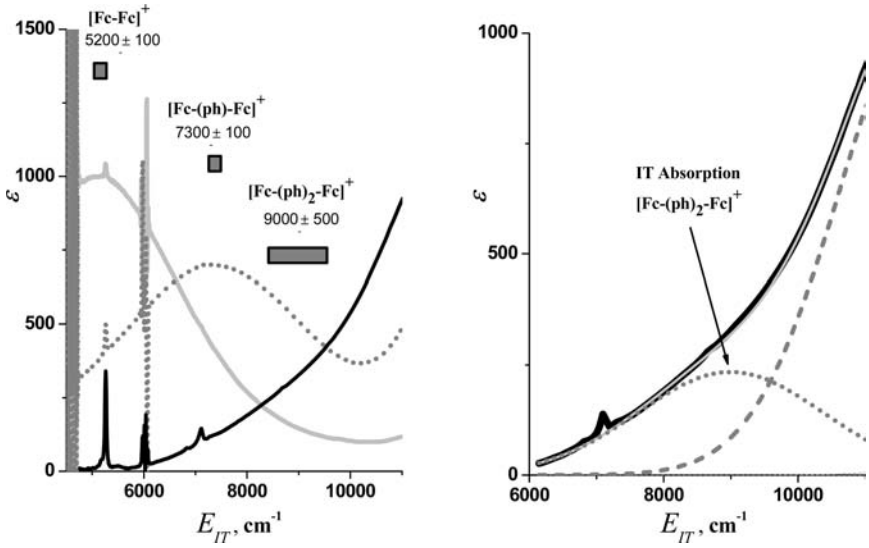

Figure 4. Intervalence absorption of the $[Fc-(ph)_n-Fc]^+$ complexes in nitrobenzene. Absorption curves in the left panel for the $[Fc-(ph)_n-Fc]^+$ series: $[Fc-Fc]^+$, gray solid; $[Fc-(ph)-Fc]^+$, gray dot; $[Fc-(ph)_2-Fc]^+$, dark solid. The spectral deconvolutions in the right panel for the $[Fc-(ph)_2-Fc]^+$ ion are as follows: the observed spectrum, dark solid; the sum of Gaussian components, gray line; the Gaussian components, dotted and dashed lines. The fit component of intervalence−valence maximum for $[Fc-(ph)_2-Fc]^+$ is 9000 ± 500 cm^{-1}.

Table 4. Basic Properties and Parameters of $[(et\text{-}Fcpy)Ru(NH_3)_4(L)]^{3+}$ and $[(et\text{-}Fcpy)_2Ru(NH_3)_4]^{3+}$.[a,b]

	$[(et\text{-}Fcpy)Ru(NH_3)_5]^{3+}$ [c]					$[(et\text{-}Fcpy)Ru(NH_3)_4(py)]^{3+}$					$[(et\text{-}Fcpy)_2Ru(NH_3)_4]^{3+}$				
solvent	$E_{IT(a)}(\varepsilon_{max})$ $[\Delta\upsilon_{1/2}]$	$H_{DA(u)}$	$\alpha^2 \times 10^2$	$-\varepsilon_s$	$\Delta G_a^{\ddagger}$	$E_{IT(a)}(\varepsilon_{max})$ $[\Delta\upsilon_{1/2}]$	$H_{DA(u)}$	$\alpha^2 \times 10^2$	$-\varepsilon_s$	$\Delta G_a^{\ddagger}$	$E_{IT(a)}(\varepsilon_{max}/Fe^{II})$,[d,e] $[\Delta\upsilon_{1/2}]$	$H_{DA(u)}$	$\alpha^2 \times 10^2$	$-\varepsilon_s$	$\Delta G_a^{\ddagger}$
DMSO	11.2(0.44) [4.09]	0.37	0.11	12	4.8	9.82(0.64) [3.92]	0.41	0.17	17	3.3	9.65(0.57)[d] [3.65]	0.37	0.15	14	3.5
DMA	11.0(0.48) [4.17]	0.39	0.13	14	4.8	9.60(0.58) [3.91]	0.39	0.17	16	3.4	9.47(0.70)[d] [3.60]	0.41	0.19	18	3.5
DMF	11.0(0.42) [4.43]	0.38	0.12	13	4.5	9.52(0.57) [4.01]	0.39	0.17	16	3.0	9.35(0.71)[d] [3.68]	0.41	0.19	18	3.3
2-butanone						7.58(0.77) [4.04]	0.40	0.28	21	1.9	7.64(1.0)[d] [4.01]	0.46	0.36	28	2.2
CH_3OH	9.27(0.64) [4.05]	0.41	0.20	18	2.9										
acetone	9.36(0.68) [4.00]	0.42	0.20	19	3.0	7.90(0.83) [4.19]	0.44	0.31	25	2.0	7.79(1.00)[d] [3.99]	0.46	0.35	27	2.2
propionitrile						7.19(0.85) [4.38]	0.43	0.36	26	1.7	7.34(1.15)[d] [3.96]	0.48	0.43	31	1.8
PC[f]	8.79(0.67) [3.87]	0.40	0.21	18	2.8	7.19(0.84) [4.27]	0.42	0.34	25	1.8	7.27(1.00)[d] [3.91]	0.44	0.37	27	1.9
acetonitrile	8.55(0.78) [3.81]	0.42	0.24	21	2.5	7.30(0.90) [4.27]	0.44	0.36	27	1.7	7.23(1.16)[d] [3.82]	0.47	0.42	31	1.7
benzonitrile	8.31(0.83) [3.86]	0.43	0.27	22	2.4	6.56(0.93) [4.00]	0.41	0.39	26	1.6	6.61(1.43)[d] [4.02]	0.51	0.60	39	1.5
nitrobenzene	6.76(0.91) [3.90]	0.41	0.37	25	1.8	7.06[g](0.70) [3.98]	0.37	0.28	19	2.0	6.40[h] (1.35)[e] [4.13]	0.50	0.61	39	1.9
nitromethane	6.72(1.02) [4.22]	0.45	0.45	30	1.6	7.80[g](0.62) [3.65]	0.35	0.20	16	2.3	7.40[h] (0.86)[e] [4.10]	0.42	0.32	24	2.3

[a] $E_{IT(a)}$, $\Delta\upsilon_{1/2}$, $H_{DA(u)}$, and $\Delta G_a^{\ddagger}$ in $cm^{-1}/10^3$; ε_{max} in M^{-1} $cm^{-1}/10^3$; $-\varepsilon_s$ in cm^{-1}. [b] The corrected ε_{max} incorporates the uncertainty on K_c, ref 29. K_c is calculated from $\Delta E_{1/2(1)}$ of Table 1. The stability energy ($-\varepsilon_s$) is calculated using eq 6. [c] Reference 36. [d] $\varepsilon_{max}/Fe^{II} = \varepsilon_{max}/2$; ε_{max} includes twice the intensity of optical transfer from $Fe^{II}-Ru^{III}$ to $Fe^{III}-Ru^{II}$ in various solvents excluding nitrobenzene and nitromethane. [e] $\varepsilon_{max}/Fe^{II} = \varepsilon_{max}$ of optical transfer from $Fe^{III}-Ru^{II}$ to $Fe^{II}-Ru^{III}$ in nitrobenzene and in nitromethane. [f] Propanediol-(1,2)-carbonate. [g] Low-energy state of $Fe^{III}-Ru^{II}$. [h] Low-energy state of $Fe^{III}-Ru^{II}-Fe^{II}$.

were 63, 15, and 2 cm^{-1} for $n = 0$, 1, and 2, respectively. However, the very low $-\varepsilon_s$ calculated for $[Fc-(ph)_2-Fc]^+$ indicates a small contribution of $-\Delta G_r$ to $-\Delta G_c$. Finally, the $[Fc-(ph)_2-Fc]^+$ cation had a very small configurational mixing parameter[1,6] ($\alpha^2 = (H_{DA}/E_{IT})^2 = 0.02\%$) between the degenerate states, $Fe^{II}-Fe^{III}/Fe^{III}-Fe^{II}$. The basic parameters of $[Fc-(ph)_2-Fc]^+$ in the two-state model are the basis for the representation of the terminal $Fe^{II}-Fe^{III}/Fe^{III}-Fe^{II}$ pair of the $[(et\text{-}Fcpy)_2Ru(NH_3)_4]^{4+}$ cation in the diabatic three-state model. Computed results of mixed-valence structures for the two-state model of the $[Fc-(ph)_2-Fc]^+$ ion show an H_{DA} between $Fe^{II}-Fe^{III}$ and $Fe^{III}-Fe^{II}$ in the PE plot in Figure S6 (Supporting Information). Apparently, the computed H_{DA}, 710 cm^{-1}, of the $[Fc-(ph)_2-Fc]^+$ ion in a vacuum is greater than the H_{DA}, 140 cm^{-1}, calculated from the experimental data using eq 1.

2. Di- and Trimetal $[(R\text{-}Fcpy)Ru(NH_3)_4L]^{3+}$ and $[(et\text{-}Fc)_2Ru(NH_3)_4]^{3+}$ Cations. In our early studies of $[(Fcpy)Ru(NH_3)_5]^{3+}$ in various solvents,[35] the upper limit of λ_o was approximately 2100 cm^{-1} and λ_i was ≈4300 cm^{-1} when a continuum dielectric approximation was used for the medium (eqs 3 and 4). The plot of λ versus $1/D_{OP} - 1/D_S$, shown in Figure S7 (Supporting Information), for $[(et\text{-}Fcpy)Ru(NH_3)_5]^{3+}$, $[(et\text{-}Fcpy)Ru(NH_3)_4(py)]^{3+}$, and $[(et\text{-}$

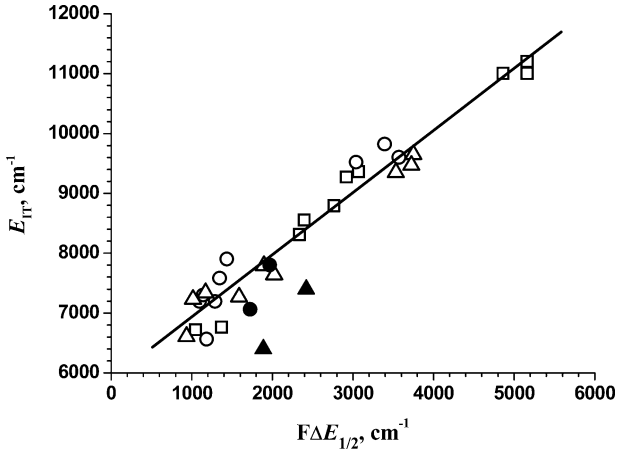

Figure 5. The E_{IT} vs $F\Delta E_{1/2}$ in various solvents for $[(et\text{-}Fcpy)Ru(NH_3)_5]^{3+}$ (open square), $[(et\text{-}Fcpy)Ru(NH_3)_4(py)]^{3+}$ (open circle), and $[(et\text{-}Fcpy)_2Ru(NH_3)_4]^{3+}$ (open triangle). The slope, intercept, and correlation coefficient (R^2) of the least-squares line without the $[(et\text{-}Fcpy)Ru(NH_3)_4(py)]^{3+}$ and $[(et\text{-}Fcpy)_2Ru(NH_3)_4]^{3+}$ in nitromethane and nitrobenzene (solid circle and triangle) were 1.04 ± 0.04, 5900 ± 120 cm^{-1}, and 0.96, respectively.

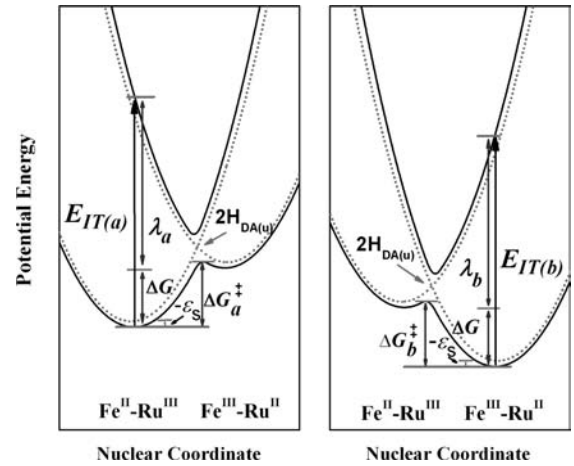

Figure 6. Qualitative illustration of basic parameters in an unsymmetric class II model. The left panel represents the basis for intervalence transfer for $[(et\text{-}Fcpy)Ru(NH_3)_5]^{3+}$ and $[(et\text{-}Fcpy)Ru(NH_3)_4(py)]^{3+}$ in various solvents, excluding the $[(et\text{-}Fcpy)Ru(NH_3)_4(py)]^{3+}$ in nitro-based solvents. Intervalence-transfer behaviors of $[(et\text{-}Fcpy)Ru(NH_3)_4(py)]^{3+}$ in nitrobenzene and nitromethane are shown in the right panel. The potential curves for the diabatic limit (dotted curves) and configurational mixing between donor and acceptor states (solid curves) are shown in both panels.

$Fcpy)_2Ru(NH_3)_4]^{3+}$ in various solvents gave small ranges of λ_o of 2100, 2600, and 1800 cm^{-1}, respectively, and λ_i of 4300, 3900 and 4400 cm^{-1}, respectively. The range of solvent reorganizational contributions to optical IT energies of the [ferrocene−rutheniumam(m)ine(III)]$^{3+}$ series is less than the λ_o of some classic weak-coupling systems, implying that the DA coupling of the [ferrocene−rutheniumam(m)ine(III)]$^{3+}$ series is relatively significant. For example, the solvent reorganizational energies of $[Ru(NH_3)_4(bpy)]^{2+}/[Ru(NH_3)_4(bpy)]^{3+}$ self-exchange in water (bpy = 2,2′-bipyridine) and the range of λ_o for Fc^+/Fc^0 self-exchange in various solvents are approximately 10500 cm^{-1} [70] and 8700 cm^{-1},[68,69] respectively. In addition, the range of solvent reorganizational contributions to E_{IT} of $[\{Ru(NH_3)_5\}_2(4,4'\text{-bipyridine})]^{5+}$ in various solvents is approximately 7000 cm^{-1}.[6]

The optical energy of intervalence transfer (E_{IT}) for the unsymmetric class II type complexes contains the reorganization energy (λ) and the free energy difference (ΔG) between the minima of the donor and acceptor states[1,6]

$$E_{IT} = \lambda + \Delta G \approx \lambda + F\Delta E_{1/2} \qquad (10)$$

where $\Delta E_{1/2}$ is the measured half-wave potential difference between the two metal centers and F is the Faraday constant. For optical transfer, the PE plots of unsymmetric mixed-valence complexes of $[(R\text{-}Fcpy)Ru(NH_3)_5]^{3+}$ show a solvent-insensitive $Fe^{II}-Ru^{III}$ state and a solvent-tunable $Fe^{III}-Ru^{II}$ state.[35,36] The least-squares fit of E_{IT} versus $F\Delta E_{1/2}$ for the $[(R\text{-}Fcpy)Ru(NH_3)_5]^{3+}$, where R= H, ethyl, Br, and acety-, in various solvents yields $\lambda \approx 0.74 \pm 0.04$ eV $\approx$ 6000 cm^{-1}.[36] The influence of both D.N.[37] and the substituent effect (σ_p)[71] on the intervalence transfer energy of the $[(R\text{-}Fcpy)Ru(NH_3)_5]^{3+}$ series was described in our early work.[36]

On the basis of eq 10, Figure 5 shows an E_{IT} versus $F\Delta E_{1/2}$ plot for the various mixed-valence complexes in most solvents studied. The overall least-squares fit in Figure 5 is $E_{IT} \approx (5900 \pm 120) + (1.04 \pm 0.04) \times F\Delta E_{1/2}$ cm^{-1}, and the reorganization energy is 5900 ± 120 cm^{-1}. The smaller reorganization energy based on the intercept of the E_{IT} versus $F\Delta E_{1/2}$ plot (Figure 5) compared with the weakly coupled limit suggests that (a) the effective distance between the donor and acceptor is less than the distance between metal centers, (b) DA configurational mixing is more significant than the H_{DA}-underestimated eq 1, and (c) the factors that contribute to $E_{1/2}$ may not be the same as those that contribute to E_{IT}.

Two two-state types of unsymmetric class II representations for $[(et\text{-}Fcpy)Ru(NH_3)_4(L)]^{3+}$ and $[(et\text{-}Fcpy)_2\text{-}Ru(NH_3)_4]^{3+}$ ions in various solvents, where L = py or NH_3, are shown in Figure 6. Some of the energy terms shown in Figure 6 were described in detail, such as $\lambda_a \approx 6000$ cm^{-1}, as were the effects of solvent donicity on ΔG. The activation energy, $\Delta G^{\ddagger}_a$, of thermal electron-transfer for $[(et\text{-}Fcpy)Ru(NH_3)_5]^{3+}$ and $[(et\text{-}Fcpy)Ru(NH_3)_4(py)]^{3+}$ in various solvents can be described, as follows:[1,6]

$$\Delta G^{\ddagger}_a = \frac{(\lambda + \Delta G)^2}{4\lambda} - H_{DA} \approx \frac{(E_{IT})^2}{4(E_{IT} - F\Delta E_{1/2(1)})} - H_{DA} \qquad (11)$$

where $\Delta E_{1/2(1)} = E_{1/2(1)}(Fe^{III/II}) - E_{1/2}(Ru^{III/II})$, as shown in Table 1. The calculated $\Delta G^{\ddagger}_a$ of the ground-state curve for $[(et\text{-}Fcpy)\text{-}Ru(NH_3)_5]^{3+}$ in various solvents ranged between 4800 and 1580 cm^{-1}, and the decrease in $\Delta G^{\ddagger}_a$ was relative to the decreased ΔG between the minima of the reactant and product.[36] Similarly, the calculated $\Delta G^{\ddagger}_a$ of $[(et\text{-}Fcpy)Ru(NH_3)_4(py)]^{3+}$ and $[(et\text{-}Fcpy)_2Ru(NH_3)_4]^{3+}$ in the various solvents, except for nitro-based solvents, ranged between 3400 and 1600 cm^{-1} and 3500 and 1500 cm^{-1}, respectively, and are summarized in Table 4. On the basis

(70) Endicott, J. F. In *Comprehensive Cooedination Chemistry II*; McCleverty, J., Meyer, T. J., Eds.; Pergamon: Oxford, U.K., 2003; Vol. 7, p 657.

(71) Muroy, S. L.; Carmichael, I.; Hug, G. L. *Handbook of Photochemistry*; Marcel Dekker: New York, 1993.

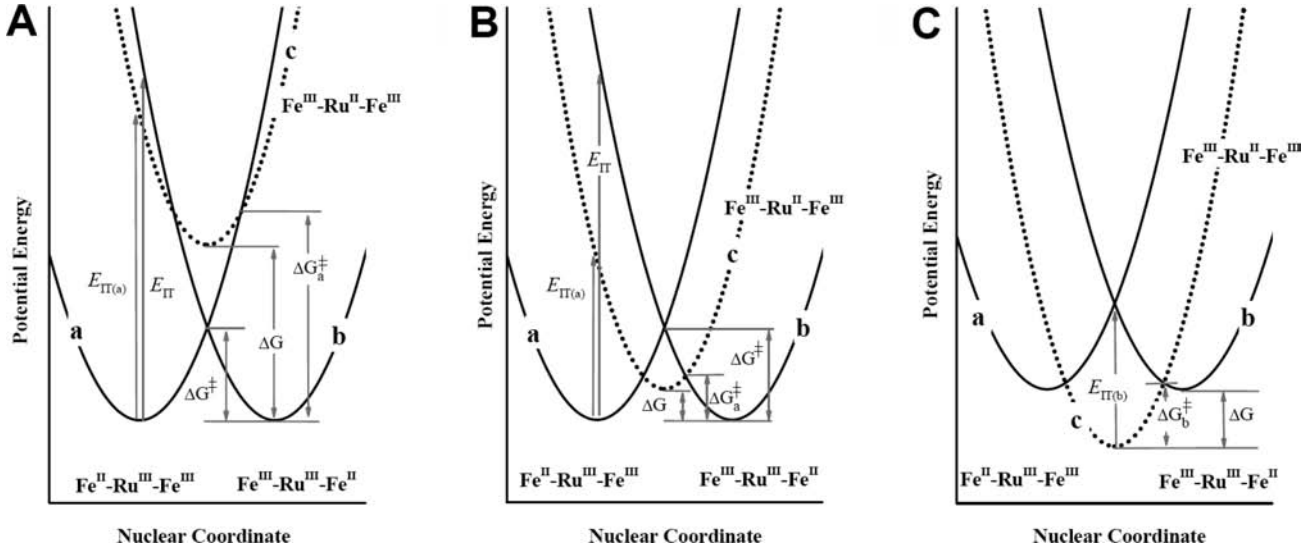

Figure 7. Qualitative illustrations of the intervalence transfer for a $[(et\text{-}Fcpy)_2Ru(NH_3)_4]^{4+}$ cation in various solvents. The diabatic-limit PE curves illustrate the energy relationships for the terminally degenerate states ($Fe^{II}-Ru^{III}-Fe^{III}/Fe^{III}-Ru^{III}-Fe^{II}$, solid curves, the a and b states) and a mediating state ($Fe^{III}-Ru^{II}-Fe^{III}$, dashed curve, the c state) in each panel. Panel A is a qualitative illustration of $[(et\text{-}Fcpy)_2Ru(NH_3)_4]^{4+}$ in DMSO, DMA, and DMF. Panel B shows $[(et\text{-}Fcpy)_2Ru(NH_3)_4]^{4+}$ in propionitrile, PC, acetonitrile, and benzonitrile. Panel C depicts $[(et\text{-}Fcpy)_2Ru(NH_3)_4]^{4+}$ in nitrobenzene and nitromethane.

of the results of both the electrochemical studies and the absorption spectra for $[(et\text{-}Fcpy)Ru(NH_3)_4(py)]^{3+}$ and $[(et\text{-}Fcpy)_2Ru(NH_3)_4]^{3+}$, the optical intervalence transfer in various solvents results in the transfer from the $Fe^{II}-Ru^{III}$ state to the $Fe^{III}-Ru^{II}$ state. In contrast, the intervalence transfer in nitromethane and nitrobenzene results in the opposite transfer of $Fe^{III}-Ru^{II}$ to $Fe^{II}-Ru^{III}$. In addition, the theoretical parameters of the two-state model for $[(et\text{-}Fcpy)Ru(NH_3)_4(py)]^{3+}$ and $[(et\text{-}Fcpy)_2Ru(NH_3)_4]^{3+}$ in nitro-based solvents are illustrated qualitatively in the right panel of Figure 6.

The $H_{DA(u)}$ of $[(et\text{-}Fcpy)Ru(NH_3)_5]^{3+}$ in various solvents ranged between 370 and 450 cm^{-1}. Similarly, the $H_{DA(u)}$ of $[(et\text{-}Fcpy)Ru(NH_3)_4(py)]^{3+}$ and $[(et\text{-}Fcpy)_2Ru(NH_3)_4]^{3+}$ in various solvents, excluding nitro-based solvents, ranged between 390 and 440 cm^{-1} and 370 and 510 cm^{-1}, respectively. Configurational mixing between the donor state ($Fe^{II}-Ru^{III}$) and acceptor state ($Fe^{III}-Ru^{II}$) of $[(et\text{-}Fcpy)Ru(NH_3)_5]^{3+}$, $[(et\text{-}Fcpy)Ru(NH_3)_4(py)]^{3+}$, and $[(et\text{-}Fcpy)_2Ru(NH_3)_4]^{3+}$ resulted in stabilization of the ground state, calculated using eq 6. For $[(et\text{-}Fcpy)Ru(NH_3)_5]^{3+}$, the $-\varepsilon_s$ of donor state ($Fe^{II}-Ru^{III}$) ranged between 15 and 30 cm^{-1} in various solvents. For $[(et\text{-}Fcpy)Ru(NH_3)_4(py)]^{3+}$ and $[(et\text{-}Fcpy)_2Ru(NH_3)_4]^{3+}$, the $-\varepsilon_s$ of ground state ($Fe^{II}-Ru^{III}$) ranged between 16 and 27 cm^{-1} and 14 and 39 cm^{-1} in various solvents, excluding nitro-based solvents, respectively. The calculated $-\varepsilon_s$ for $[(et\text{-}Fcpy)Ru(NH_3)_4(L)]^{3+}$ and $[(et\text{-}Fcpy)_2Ru(NH_3)_4]^{3+}$ in various solvents showed small amplitudes on the PE scale, as illustrated in the left panel of Figure 6. The relative parameters of intervalence charge-transfer properties for the $[(et\text{-}Fcpy)Ru(NH_3)_4(L)]^{3+}$ and $[(et\text{-}Fcpy)_2Ru(NH_3)_4]^{3+}$ ions are summarized in Table 4.

3. Three-State Model for the Intervalence Transfer of the $[(et\text{-}Fcpy)_2Ru(NH_3)_4]^{4+}$ Cation. Conceivably, the important points of our interpretation of the mixed-valence properties of $[(et\text{-}Fcpy)_2\text{-}Ru(NH_3)_4]^{4+}$ are as follows: (a) electronic coupling between the terminally degenerate states, $Fe^{II}-Ru^{III}-Fe^{III}/Fe^{III}-Ru^{III}-Fe^{II}$, is weak (on the basis of the observed H_{DA} of $[Fc-(ph)_2-Fc]^+$); (b) two relatively strong coupling pairs between the terminal and reduced-bridge states exist ($Fe^{II}-Ru^{III}-Fe^{III}/Fe^{III}-Ru^{II}-Fe^{III}$ and $Fe^{III}-Ru^{III}-Fe^{II}/Fe^{III}-Ru^{II}-Fe^{III}$); and (c) the tunable $Fe^{III}-Ru^{II}-Fe^{III}$ state, evident in the PE plot, that results from solvent donicity is key for end-to-end interaction observed during the electrochemical studies in nitriles. Before discussing comproportionation properties of the $[(et\text{-}Fcpy)_2Ru(NH_3)_4]^{4+}$ cation in various solvents, three-state models must be described by the detailed relationships between the terminal and mediating states. The three types of the three-state model for $[(et\text{-}Fcpy)_2Ru(NH_3)_4]^{4+}$ in various solvents are shown in Figure 7. The diabatic limits of the three types of three-state model are as follows: (a) the $\Delta G > \Delta G^{\ddagger}$ of a three-state model with a relatively high energy of the reduced-bridge state is classified as type A (ΔG = the free-energy difference between the minima of the degenerate states and the reduced-bridge state, $\Delta G^{\ddagger}$ = the activation energy between degenerate states); (b) the $\Delta G < \Delta G^{\ddagger}$ of a three-state model with a relatively low-energy mediating state is classified as type B, and (c) a three-state model with the lowest-energy state of the reduced-bridge state is classified as type C. For types A, B, and C of $[(et\text{-}Fcpy)_2Ru(NH_3)_4]^{4+}$ in various solvents, some basic energy terms of the mixed-valence properties between the terminal and reduced-bridge states of $[(et\text{-}Fcpy)_2Ru(NH_3)_4]^{4+}$, $E_{IT(a)}$, $H_{DA(u)}$, ΔG, and $\Delta G^{\ddagger}_a$, should be similar to the properties between the $Fe^{II}-Ru^{III}$ and $Fe^{III}-Ru^{II}$ states of $[(et\text{-}Fcpy)Ru(NH_3)_4(py)]^{3+}$ and of $[(et\text{-}Fcpy)_2Ru(NH_3)_4]^{3+}$ in the weak coupling limit. In addition, the properties between degenerate states should be similar to the properties of $[Fc-(ph)_2-Fc]^+$.

In contrast, the reorganizational energy ($\lambda = E_{IT} \approx 9000$ cm^{-1}) of $[Fc-(ph)_2-Fc]^+$ is well-resolved in the reorgani-

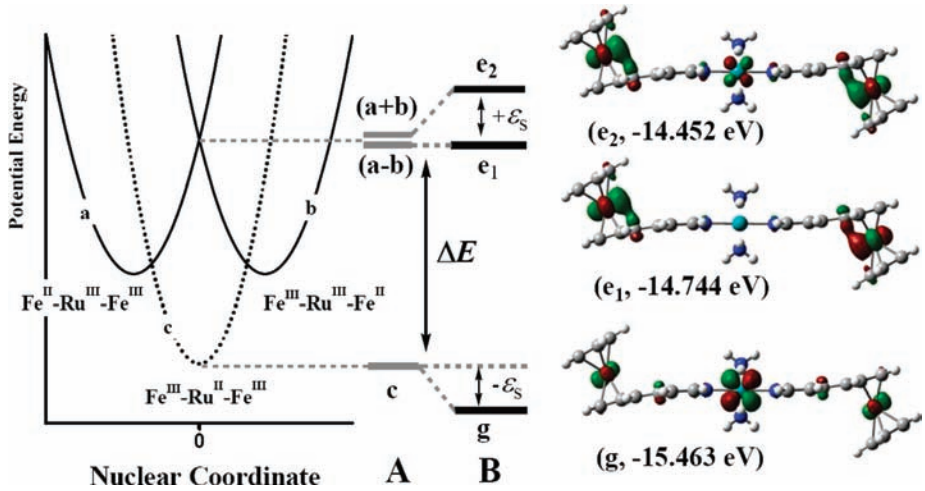

Figure 8. For the covalently linked $[(et\text{-}Fcpy)_2Ru(NH_3)_4]^{4+}$ ion. Qualitative illustrations of the type C model for the computed results represent the select orbital structures at the origin nuclear coordinate in the C_{2h} group. The diabatic limits are represented by step A, and the adiabatic states are shown in step B. In step A, the degenerate states, a and b, at the origin nuclear coordinate include a symmetric (a + b) and an antisymmetric (a − b) combination. In step B, the configurational mixing between g and e_2 at the origin implied significant coupling between a dπ orbital of central Ru(II) and the orbital of symmetric combination of the terminal $Fe^{II}-Fe^{III}/Fe^{III}-Fe^{II}$ couple.

zational energy between the terminally degenerate states of $[(et\text{-}Fcpy)_2Ru(NH_3)_4]^{4+}$ in types A and B, as shown in Figure 7. Thus, the approximate activation energy ($\Delta G^{\ddagger} \approx \lambda/4$) of $[(et\text{-}Fcpy)_2\text{-}Ru(NH_3)_4]^{4+}$ between degenerate states in the diabatic limit is approximately 2300 cm^{-1}. On the basis of $\Delta G^{\ddagger} \approx 2300$ cm^{-1} and $\Delta G \approx F\Delta E_{1/2(1)}$ for $[(et\text{-}Fcpy)_2Ru(NH_3)_4]^{4+}$ in types A and B, the following conclusions can be drawn: $\Delta G > \Delta G^{\ddagger}$ is type A in DMSO, DMA, and DMF ($\Delta G \approx 3800$, 3700, and 3500 cm^{-1}, respectively); $\Delta G < \Delta G^{\ddagger}$ is type B in propionitrile, PC, acetonitrile, and benzonitrile ($\Delta G \approx 1200$, 1600, 1000 and 900 cm^{-1}, respectively); and the reasonable model in 2-butanone and acetone is situated between types A and B ($\Delta G \approx 2000$, 1900 cm^{-1}, respectively; the ΔG is too closed to $\Delta G^{\ddagger}$). The basis of $E_{1/2}(Ru^{III/II}) > E_{1/2}(Fe^{III/II})$ for $[(et\text{-}Fcpy)_2Ru(NH_3)_4]^{4+}$ in nitro-based solvents suggests that the intervalence-transfer three-state model for $[(et\text{-}Fcpy)_2Ru(NH_3)_4]^{4+}$ is type C. Some usefully computational features with the type C model for the $[(et\text{-}Fcpy)_2Ru(NH_3)_4]^{4+}$ are shown in Figure 8. The effective mixing between g and e_2 at the origin is the cause of the large $-\varepsilon_s$ (0.292 eV = 2400 cm^{-1}). The coupling, $H_{(ab)\text{-}c}$, of the computational results between the mediating state (c state) and the combination state of the terminal states (a and b states) is approximately 2900 cm^{-1} ($\Delta E = 0.427$ eV = 3400 cm^{-1}, $-\varepsilon_s = (H_{(ab)\text{-}c})^2/\Delta E$). The computed value of $H_{(ab)\text{-}c}$, which is apparently too strong, implies that significant coupling mediates the end-to-end interaction of the $Fe^{II}-Fe^{III}/Fe^{III}-Fe^{II}$ couple.

4. Issues Regarding the Comproportionation Terms. The free energy of comproportionation, ΔG_c, for the mixed-valence dimetal complexes includes the following components: statistical distribution of the comproportionation equilibrium (ΔG_s), electrostatic repulsion between the two metal-ion centers (ΔG_e), the inductive factor (ΔG_i), the resonance effect (ΔG_r), and the electron-exchange contributions (ΔG_{ex}).[10,24,25,40] In weakly coupled systems, the limit of the relevant comproportionation constant is 4 ($-\Delta G_c =$ 290 cm^{-1}).[6,24,25] The electrochemical studies of $[(et\text{-}Fcpy)_2Ru(NH_3)_4]^{2+}$ in DMSO, DMA, DMF, 2-butanone, acetone, and PC ($\Delta E_{1/2(2)} \leq 70$ mV, $\Delta E_{1/2(2)} = E_{1/2(second)}(Fe^{III/II}) - E_{1/2(first)}(Fe^{III/II})$, $K_c \leq 15$) suggest that K_c ($-\Delta G_c$) ranges from 4 to 15 (290 to 560 cm^{-1}). However, when the solvent stabilizes the +3 oxidation state of the Ru center, relatively large values of $-\Delta G_c$ are observed for $[(et\text{-}Fcpy)_2Ru(NH_3)_4]^{4+}$ in propionitrile, acetonitrile, and benzonitrile (670, 790, and 870 cm^{-1}, respectively), suggesting that some unique energy factor contributes to $-\Delta G_c$. We evaluated the $-\Delta G_e$ of $[(et\text{-}Fcpy)_2Ru(NH_3)_4]^{4+}$ between terminal centers, using the equation $-\Delta G_e = [Q_iQ_j - Q_i(Q_j + 1)]/(4\pi\varepsilon_{sol}\varepsilon_o r)$,[41] where Q_i, Q_j, and $Q_j + 1$ are the (2+, 2+/2+, 3+) charge couple of terminal $Fe^{3+/2+}$ centers, r represents the separation of the terminal centers (15.8 Å), ε_{sol} depicts the static dielectric of the solvent, and ε_o is the permittivity of free space. A further problem is that the expression of $-\Delta G_e$ is appropriate for a complex in pure solution, but it is not very relevant to an electrochemical measurement of a complex in a 0.1 M electrolyte solution. Therefore, it offers only qualitative explanation for the effect of $-\Delta G_e$ on $-\Delta G_c$. The values of $-\Delta G_e$ calculated for $[(et\text{-}Fcpy)_2Ru(NH_3)_4]^{4+}$ in various solvents were 80 (DMSO), 95 (DMA), 95 (DMF), 200 (2-butanone), 180 (acetone), 125 (propionitrile), 55 (PC), 105 (acetonitrile), and 145 cm^{-1} (benzonitrile). However, depending on the solvent, $-\Delta G_e$ ranged between 55 and 200 cm^{-1}, and the extreme values of $-\Delta G_e$ were 55 (PC) and 200 cm^{-1} (2-butanone). The unremarkable $-\Delta G_e$ values for $[(et\text{-}Fcpy)_2Ru(NH_3)_4]^{4+}$ in nitriles do not fully explain the unusual $-\Delta G_c$ values of $[(et\text{-}Fcpy)_2Ru(NH_3)_4]^{4+}$ in nitriles. The $-\Delta G_r$ of $[(et\text{-}Fcpy)_2Ru(NH_3)_4]^{4+}$ in types A and B of Figure 7 can be calculated from the sum of the stabilization energy ($-\varepsilon_s$) of configurational mixing between terminal a and b states ($-\varepsilon_{s(s)}$) and between mediating and terminal states ($-\varepsilon_{s(a)}$) using the classical two-state model:

$$-\Delta G_r = -2\varepsilon_s = -2(\varepsilon_{s(s)} + \varepsilon_{s(a)}) \quad (12)$$

The appreciable components of $-\varepsilon_s$ for $[(et\text{-}Fcpy)_2Ru(NH_3)_4]^{4+}$ approached $-\varepsilon_{s(s)} \approx -\varepsilon_s$ of $[Fc-(ph)_2-Fc]^+$ and $-\varepsilon_{s(a)} \approx -\varepsilon_s$ of $[(et\text{-}Fcpy)Ru(NH_3)_4(py)]^{3+}$ and $[(et\text{-}Fcpy)_2Ru(NH_3)_4]^{3+}$. Therefore, possible $-\Delta G_r$ values of $[(et\text{-}Fcpy)_2Ru(NH_3)_4]^{4+}$ ranged between 32 and 82 cm^{-1} in various solvents with D.N. between 29.8 and 11.9. However, $-\Delta G_r$'s that are based on the classical model do not make a significant contribution to the relatively large $-\Delta G_c$ of $[(et\text{-}Fcpy)_2Ru(NH_3)_4]^{4+}$ in nitriles, where the extra energy components of $-\Delta G_c$ ($-\Delta G_{c(extra)}$, $-\Delta G_{c(extra)} \geq -\Delta G_c - 560$ cm^{-1}) in propionitrile, acetonitrile, and benzonitrile were greater than or equal to 110, 230, and 310 cm^{-1}, respectively. In addition to the contributions of $-\Delta G_e$ and $-\Delta G_r$, $-\Delta G_{ex}$ likely affects $-\Delta G_{c(extra)}$, and $-\Delta G_{ex}$ contains the antiferromagnetic-exchange factor.[15] The calculated stabilization-energy term of antiferromagnetic exchange ($-J_{af(calcd)}$) can be evaluated using the equation developed by Bertrand as follows:[42]

$$-J_{af(calcd)} = \frac{2(H_{DA(u)})^2}{E_{IT(a)}} \quad (13)$$

The $-J_{af(calcd)}$ of $[(et\text{-}Fcpy)_2Ru(NH_3)_4]^{4+}$ between the terminal Fe^{III} and bridging Ru^{III} in various solvents is limited to a narrow range between 28 and 78 cm^{-1}. Thus, $-J_{af(calcd)}$ may not be a significant contributor to $-\Delta G_{c(extra)}$ for $[(et\text{-}Fcpy)_2Ru(NH_3)_4]^{4+}$ in nitriles. The calculated energy components of the free energy comproportionation are summarized in Table 5. In contrast, the superexchange contribution to $-\Delta G_{c(extra)}$ is the most likely explanation for the unusual $-\Delta G_c$ for $[(et\text{-}Fcpy)_2Ru(NH_3)_4]^{4+}$ in nitriles.

5. Effects of the Superexchange Coupling in the Type B Model. Regarding the phenomenon of theoretical superexchange coupling (H^s_{DA}) in the three-state system, the significant articles by Creutz, Newton, and Sutin focused on H^s_{DA} with the following limits: $H_{DA(s)} = 0$, $H_{DA(u)} > 0$, and $E_{IT(s)} \gg E_{IT(a)}$ (where $H_{DA(s)}$ = matrix element between degenerate states, $H_{DA(u)}$ = matrix element between the degenerate states and the mediating state, $E_{IT(s)}$ = intervalence energy between degenerate states, and $E_{IT(a)}$ = intervalence energy between the degenerate states and the mediating state).[7,8,20] In addition, a system developed by Crutchley focused on H^s_{DA} in the hole-transfer mechanism,[15,40] and Endicott et al. described the H^s_{DA} of end-to-end coupling with the perturbation arguments in a trimetal system.[13,14,47] For the type B model in Figure 7, the couplings between the mediating state and each of the degenerate states are equal ($H_{DA(u)} \equiv H_{ac} = H_{bc}$); the coupling between the terminal states ($H_{DA(s)} \equiv H_{ab}$) is zero. Under these conditions, the effective superexchange coupling between terminal states can be given by[20,47]

$$H^s_{DA} = \frac{H_{ac}H_{bc}}{\Delta E_{ave}} \quad (14)$$

where E_{ac} and $E_{bc} \gg H_{ac}$, $\Delta E_{ave} = 2E_{ac}E_{bc}/(E_{ac}+E_{bc})$, and $E_{ac} = E_{IT(a)}$ and $E_{bc} = E_{IT} - E_{IT(a)} \approx 10000$ $cm^{-1} - E_{IT(a)}$ (E_{ij} = vertical energy between the terminal and bridging states). If $H_{DA(s)} = 0$, the H^s_{DA} evaluated by eq 14 for $[(et\text{-}Fcpy)_2Ru(NH_3)_4]^{4+}$ in ketones, PC, and nitriles ranged between 49 and 61 cm^{-1} (see Table 6). We have considered that the superexchange phenomenon is treated by the distortion of the mediating state in the triangular system, but the small amplitude of the calculated H^s_{DA} ranges between 17 and 18 cm^{-1} (see Appendix A). The unremarkable calculated values of H^s_{DA} and the relatively large $\Delta G_{c(extra)}$ for $[(et\text{-}Fcpy)_2Ru(NH_3)_4]^{4+}$ in nitriles suggest the following: (a) effective $H_{DA(u)}$ is more significant than $H_{DA(u)}$ according to eq 1; (b) the factor that $H_{DA(s)}$ contributes to H^s_{DA} may not be neglected in this case; and (c) the possible sum of configurational mixing between the ground and MLCT excited states contributes to the ground-state distortion. However, there is no basis for any significant conclusions for the calculation of H^s_{DA} including $H_{DA(s)}$. For the type C model shown in Figure 8, the computed value of coupling was too large, that is, $H_{(ab)\text{-}c} \approx 2900$ cm^{-1}, between a symmetric combination of the degenerate states and the mediating state. It's possible that the reduced-bridge state mediates the end-to-end superexchange coupling for $[(et\text{-}Fcpy)_2Ru(NH_3)_4]^{4+}$ in various solvents. For $[(et\text{-}Fcpy)_2Ru(NH_3)_4]^{4+}$, the remarkable $-\Delta G_{c(extra)}$ in nitriles implies a very distorted ground-state curve, and the large computed value of $H_{(ab)\text{-}c}$ in the type C model indicated significant configurational mixing between the degenerate states and the mediating state in the type B model. The qualitative relationships of adiabatic three-state curves for $[(et\text{-}Fcpy)_2Ru(NH_3)_4]^{4+}$ in the type B model are shown in Figure 9.

In our type B model for $[(et\text{-}Fcpy)_2Ru(NH_3)_4]^{4+}$ in nitriles, we chose to study the end-to-end interaction phenomenon from the perspective of the perturbation arguments. In Figure 9, the configurational mixing between the mediating state and the ground state (a state of symmetric combination between degenerate states) signified that the superexchange coupling contributed to the distortion of the ground-state curve. The phenomenon of a relatively large $-\Delta G_c$ of $[(et\text{-}Fcpy)_2Ru(NH_3)_4]^{4+}$ in nitriles is not a source of an energy factor of comproportionation in classic conceptions, not even the term of $-\Delta G_r$ in the perturbation argument of the two-

Table 5. Components of Free Energy Comproportionation between the $Fe^{II}-Fe^{III}/Fe^{III}-Fe^{II}$ Pair for the Complexes $[(et\text{-}Fcpy)_2Ru(NH_3)_4]^{4+}$ in Various Solvents

solvents	K_c[a]	$-\Delta G_c$,[b] cm^{-1}	$-\Delta G_{c(extra)}$,[c] cm^{-1}	$-\Delta G_e$,[d] cm^{-1}	$-\Delta G_r$,[e] cm^{-1}	$-J_{af(calcd)}$,[f] cm^{-1}
DMSO	≤15, >4	≤560, >290		80	32	28
DMA	≤15, >4	≤560, >290		95	40	36
DMF	≤15, >4	≤560, >290		95	40	36
2-butanone	≤15, >4	≤560, >290		200	60	56
acetone	≤15, >4	≤560, >290		180	58	54
propionitrile	25	670	≥110	125	66	62
PC	≤15, >4	≤560, >290		55	58	54
acetonitrile	47	790	≥230	105	66	62
benzonitrile	67	870	≥310	145	82	78
nitrobenzene	≤15, >4[g]	≤560, >290[g]				
nitromethane	≤15, >4[g]	≤560, >290[g]				

[a] $K_c = 10\exp(\Delta E_{1/2(2)}/59.1)$. Data of $\Delta E_{1/2(2)}$ are in Table 1. $\Delta E_{1/2(2)}$ is in millivolts. [b] $-\Delta G_c = 207 \times \ln K_c$, cm^{-1}. [c] $-\Delta G_{c(extra)} \geq -\Delta G_c - 560$ cm^{-1}. [d] $-\Delta G_e = [Q_iQ_j - Q_i(Q_j + 1)]/(4\pi\varepsilon_{sol}\varepsilon_o r)$, ref 41 and section 4 of the Discussion. [e] $-\Delta G_r \approx -2[\varepsilon_{s(s)} + \varepsilon_{s(a)}]$. [f] Stabilization energy of the antiferromagnetic exchange, eq 13. [g] Comproportionation properties of $[(et\text{-}Fcpy)_2Ru(NH_3)_4]^{3+}$.

Table 6. Basic Energy Terms of $[\text{et-Fcpy})_2\text{Ru(NH}_3)_4]^{4+}$ in Three-State Models

solvents	$E_{IT(a)}$,[a] $cm^{-1}/10^3$	E_{IT},[b] $cm^{-1}/10^3$	ΔG,[c] $cm^{-1}/10^3$	$H_{DA(s)}$,[d] $cm^{-1}/10^3$	$H_{DA(u)}$,[e] $cm^{-1}/10^3$	$\Delta G_{(s)}^{\ddagger}$,[f] $cm^{-1}/10^3$	$\Delta G_{(a)}^{\ddagger}$,[g] $cm^{-1}/10^3$	type[h]	H_{DA}^{s},[i] cm^{-1}
DMSO	≈ 9.7	≥9.0	≈ 3.8	≤0.14	≈ 0.37	≥2.1	≈ 3.6	A	
DMA	≈ 9.5	≥9.0	≈ 3.7	≤0.14	≈ 0.41	≥2.1	≈ 3.5	A	
DMF	≈ 9.4	≥9.0	≈ 3.5	≤0.14	≈ 0.41	≥2.1	≈ 3.3	A	
2-butanone	≈ 7.6	≥9.0	≈ 2.0	≤0.14	≈ 0.46	≥2.1	≈ 2.1	A∼B	59
acetone	≈ 7.8	≥9.0	≈ 1.9	≤0.14	≈ 0.46	≥2.1	≈ 2.1	A∼B	61
propionitrile	≈ 7.3	≥9.0	≈ 1.2	≤0.14	≈ 0.48	≥2.1	≈ 1.7	B	59
PC	≈ 7.3	≥9.0	≈ 1.6	≤0.14	≈ 0.44	≥2.1	≈ 1.9	B	49
acetonitrile	≈ 7.2	≥9.0	≈ 1.0	≤0.14	≈ 0.47	≥2.1	≈ 1.6	B	55
benzonitrile	≈ 6.6	≥9.0	≈ 0.9	≤0.14	≈ 0.51	≥2.1	≈ 1.4	B	58
nitrobenzene[j]	≈ 6.4		≈ 1.9		0.50			C	
nitromethane[j]	≈ 7.4		≈ 2.4		0.42			C	

[a] $\approx E_{IT(a)}$ of $[\text{(et-Fcpy)}_2\text{Ru(NH}_3)_4]^{3+}$ in various solvents (see Table 4). [b] $\geq E_{IT}$ of $[\text{Fc}-(\text{ph})_2-\text{Fc}]^{+}$ in nitrobenzene (see Table 2). [c] $\approx F\Delta E_{1/2(1)}$ of $[\text{(et-Fc)}_2\text{-Ru}]^{2+}$ in various solvents (Table 1). [d] $H_{DA(s)}$ between terminal $Fe^{II}-Fe^{III}/Fe^{III}-Fe^{II}$ pair in two-state limit; $H_{DA(s)} \leq H_{DA}$ of $[\text{Fc}-(\text{ph})_2-\text{Fc}]^{+}$. [e] Matrix element between a terminal state and the mediating state; $\approx H_{DA(u)}$ of $[\text{(et-Fcpy)}_2\text{Ru(NH}_3)_4]^{3+}$ between $Fe^{II}-Ru^{III}/Fe^{II}-Ru^{III}$ states (Table 4). [f] $\Delta G_{(s)}^{\ddagger} = (E_{IT})^2/4 - H_{DA(s)}$. [g] $\approx \Delta G_{(a)}^{\ddagger}$ of $[\text{(et-Fcpy)}_2\text{Ru(NH}_3)_4]^{3+}$ in various solvents; $\Delta G_{(a)}^{\ddagger} = [(E_{IT(a)})^2/4(E_{IT(a)} - \Delta G)] - H_{DA(a)}$. [h] Type of three-state models in Figure 7. [i] Superexchange coupling using eq 14. [j] Low-energy state is the mediating state, $Fe^{III}-Ru^{II}-Fe^{III}$.

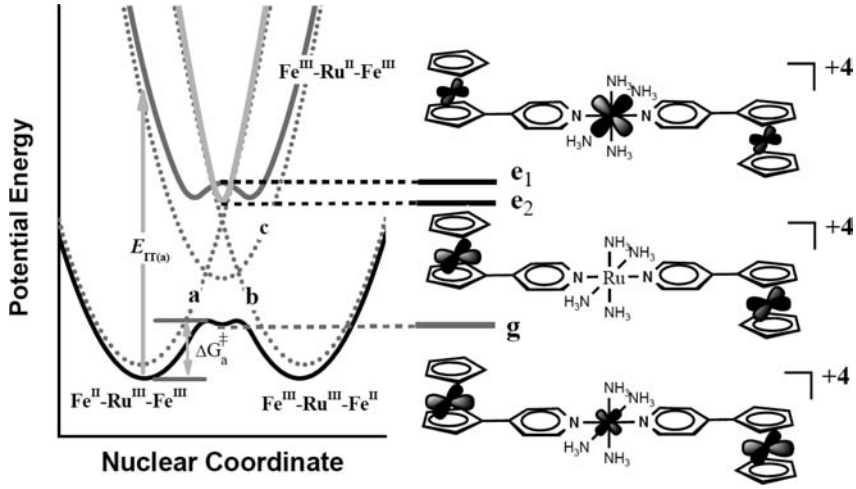

Figure 9. Qualitative PE diagram for $[\text{(et-Fcpy)}_2\text{Ru(NH}_3)_4]^{4+}$. The ethyl groups are omitted in the orbital structures, in the type B model. The solid curves illustrate the adiabatic PE curves that result from configurational mixing of the diabatic-degenerate states with the mediating state (a, b, and c shown in the dotted curves) as follows: the configurational mixing between the degenerate states and the mediating state (black and dark gray curves) and only configurational mixing between degenerate states (light gray curve). The relatively distorted low-energy curve is indicative of the reduced-bridge state mediated superexchange coupling between the degenerate states of the $Fe^{II}-Fe^{III}/Fe^{III}-Fe^{II}$ couple. The diabatic limits of the $Fe^{II}-Ru^{III}-Fe^{III}/Fe^{III}-Ru^{III}-Fe^{II}$ and $Fe^{III}-Ru^{II}-Fe^{III}$ states are shown in the dotted curves. The orbital structures in the transition-state positions of the g, e_1, and e_2 are symmetric as C_{2h} in the origin of the nuclear coordinates. The C_{2h} symmetry is at the best idealized limiting symmetry, and the molecules in solution must have lower symmetry since they are not rigid.

state model (see section 4 of the Discussion). In the argument for the third-state mediating end-to-end superexchange interaction of the $[\text{(et-Fcpy)}_2\text{Ru(NH}_3)_4]^{4+}$ system, the logical implication of the significant configurational-mixing between degenerate states and mediating state originating from efficient superexchange coupling contributed to the stabilization energy of the ground-state distortion, and the significant $-\Delta G_{c(extra)}$ of $[\text{(et-Fcpy)}_2\text{Ru(NH}_3)_4]^{4+}$ in nitriles should be the source of $-\Delta G_r$, which contains the effective superexchange-coupling, $H_{DA(eff)}^{s}$. On the basis of eqs 6 and 7 and on superexchange arguments, the equation of the probable superexchange contribution to the resonance energy ($-\Delta G_r^s$) is given by

$$-\Delta G_r^s \approx \frac{2(H_{DA(eff)}^s)^2}{\Delta E} \qquad (15)$$

where $-\Delta G_r^s \approx -\Delta G_{c(extra)}$ and the vertical ΔE between the ground and the mediating states ($\Delta E \approx E_{IT(a)}$). Reasonable estimates of the superexchange phenomenon of the end-to-end interaction for $[\text{(et-Fcpy)}_2\text{-Ru(NH}_3)_4]^{4+}$ in nitriles are as follows: $H_{DA(eff)}^{s} \approx 630$, 910, and 1000 cm^{-1} for propionitrile, acetonitrile, and benzonitrile, respectively. In addition, the calculated $-\Delta G_r^s \approx -\Delta G_{c(extra)}$ of $[\text{(et-Fcpy)}_2\text{-Ru(NH}_3)_4]^{4+}$ in nitriles increases in amplitude with decreasing $-\Delta G_a^{\ddagger}$ values for the ground-state curve between an original degenerate state and a primary mediating state, leading to the following conclusions: (a) the configurational mixing between degenerate states and the mediating state should be relatively significant and (b) future studies of end-to-end interaction involving superexchange coupling will focus on the type B model of the possible trimetal systems. On the basis of rough estimates, the superexchange contributions to the unusual value of $-\Delta G_c$ for $[\text{(et-Fcpy)}_2\text{Ru(NH}_3)_4]^{4+}$ in nitriles should be the primary reason for the significant end-to-end interactions observed in the electrochemical studies. Nevertheless, the relatively small $-\Delta G_c$ of $[\text{(et-Fcpy)}_2\text{Ru(NH}_3)_4]^{4+}$ in PC is likely caused by the very small value of $-\Delta G_e$ (55 cm^{-1}).

Conclusion

The free energy difference (ΔG) between the mixed-valence states of the $Fe^{II}-Ru^{III}/Fe^{III}-Ru^{II}$ couple in $[(et\text{-}Fcpy)Ru(NH_3)_5]^{3+}$, $[(et\text{-}Fcpy)Ru(NH_3)_4(py)]^{3+}$, and $[(et\text{-}Fcpy)_2Ru(NH_3)_4]^{3+/4+}$ demonstrated that the solvent-dependent contribution to ΔG dominates the intervalence charge-transfer energy ($E_{IT(a)}$) and reverses D/A roles in $[(et\text{-}Fcpy)Ru(NH_3)_4(py)]^{3+}$ and $[(et\text{-}Fcpy)_2Ru(NH_3)_4]^{3+/4+}$. The $\Delta E_{1/2}$ between terminal metal centers of $[(et\text{-}Fcpy)_2Ru(NH_3)_4]^{2+}$ in various solvents was less than 70 mV, but the $\Delta E_{1/2}$'s in propionitrile, acetonitrile, and benzonitrile were 83, 99, and 108 mV, respectively. The relatively large free energy of comproportionation ($-\Delta G_c$) of $[(et\text{-}Fcpy)_2Ru(NH_3)_4]^{4+}$ in nitriles suggests that the distorted PE curve of the ground state indicates effective configurational mixing between the terminal states and the mediating state. The important phenomenon reported here is the dramatic change in $\Delta E_{1/2}$ between the terminal centers of $[(et\text{-}Fcpy)_2Ru(NH_3)_4]^{2+}$, which are 15.6 Å apart, in nitriles. On the basis of the Mulliken−Hush expression, the weak H_{DA} between $Fe^{II}-Ru^{III}/Fe^{III}-Ru^{II}$ states for mixed-valence di- and trimetal complexes in various solvents ranges between 370 and 510 cm^{-1}, and the very weak H_{DA} between degenerate $Fe^{II}-Fe^{III}/Fe^{III}-Fe^{II}$ states of the $[Fc-(ph)_2-Fc]^+$ ion is less than 140 cm^{-1}. We have used the superexchange argument for the phenomenon of the relatively great $\Delta E_{1/2}$ between the elements of the terminal metal couple of the $[(et\text{-}Fcpy)_2Ru(NH_3)_4]^{2+}$ ion in nitriles, but the small amplitude of the calculated H^s_{DA} was not the key for this. In addition, the significant end-to-end interaction in the type B model for the $[(et\text{-}Fcpy)_2Ru(NH_3)_4]^{4+}$ ion in nitriles depends on the ΔG between the minima of the mediating state ($Fe^{III}-Ru^{II}-Fe^{III}$) and the degenerate states ($Fe^{II}-Ru^{III}-Fe^{III}/Fe^{III}-Ru^{III}-Fe^{II}$). The effective superexchange coupling ($H^s_{DA(eff)}$) based on the perturbation argument and the resonance free energy of comproportionation for the $[(et\text{-}Fcpy)_2Ru(NH_3)_4]^{4+}$ ion in nitriles ranges between 630 and 1,000 cm^{-1} in the extent.

Acknowledgment. The authors thank the National Science Council of R.O.C. for supporting this research (NSC-95-2113-M-030-003).

Appendix A: The Bridging-State Distortion of the Type B Model in a Triangular System

The superexchange phenomenon was treated as mediating state distortion in the early literature.[20] The type B model of the $[(et\text{-}Fcpy)_2Ru(NH_3)_4]^{4+}$ ion in three dimensions is illustrated in the left panel of Figure 10. The symmetric triangular system has been treated by Bersuker[72] and Tesukerblat,[73] but we would expect an isosceles triangular system to be more relevant. In work with the $[(et\text{-}Fcpy)_2Ru(NH_3)_4]^{4+}$ ion in nitriles, the weak H_{DA} ($H_{DA} < 140$ cm^{-1}) between degenerate states for $[Fc-(ph)_2-Fc]^+$ and

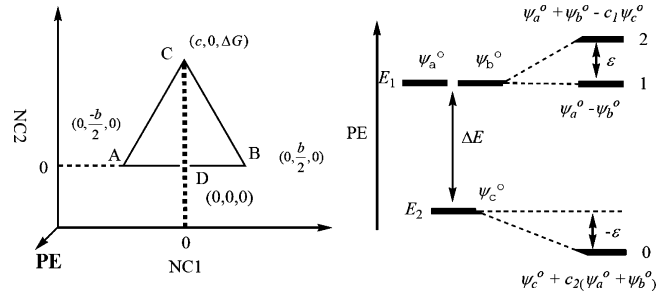

Figure 10. Qualitative illustration of the type B model of the relationships between degenerate states (a and b states with minima positions at A and B, respectively) and the bridging state (c state with relatively higher energy minimum at C, $\Delta G > 0$) for $[(et\text{-}Fcpy)_2Ru(NH_3)_4]^{4+}$ in the isosceles triangle (left panel). The view in the left panel is along the PE axis. Two general nuclear coordinates, NC1 and NC2, are antisymmetric and symmetric distortions. The basic assumptions in this system are that there is no mixing between degenerate states ($H_{ab} = 0$) and weak mixing between bridging and degenerate states (H_{ac} and $H_{bc} > 0$). At position C, ΔE is the vertical energy between c and the degenerate states in the diabatic limit, and ΔE is greater than the stabilization energy, ε.

the relatively strong coupling ($H_{DA(u)}$ ranging between 370 and 510 cm^{-1}) between the $Fe^{II}-Ru^{III}/Fe^{III}-Ru^{II}$ couple for the $[(et\text{-}Fc\text{-}py)_yRu^{III}(NH_3)_x]^{3+}$ series ($x = 4$ and $y = 2$ or $x = 5$ and $y = 1$) in various solvents indicated that the bridging state (c state) mediation of electron transfer is commonly attributed to superexchange coupling (H^s_{DA}) between degenerate states. Configurational mixing between the c state and the symmetric combination of degenerate states is illustrated by equations A1 and A2 (right panel of Figure 10, $c1 \approx c2 \equiv H_{ij}/\Delta E$):

$$\psi_0 = [\psi^o_c + c_1(\psi^o_a + \psi^o_b)]/\sqrt{[1 + 2(c_1)^2]} \qquad \text{(A1)}$$

$$\psi_2 = [\psi^o_a + \psi^o_b - c_2\psi^o_c]/\sqrt{[2 + (c_2)^2]} \qquad \text{(A2)}$$

The secular determinant for such a three-state system at the minimum bridging state can be written as in shown eq A3 (assume $E_1 = 0$, $H_{ab} = 0$, and weak coupling of $H_{ac} = H_{bc}$)

$$\begin{vmatrix} -\Delta E-\varepsilon & H_{ac} & H_{ac} \\ H_{ac} & 0 & \varepsilon \\ H_{ac} & \varepsilon & 0 \end{vmatrix} = 0 \qquad \text{(A3)}$$

The resulting secular equation is $\varepsilon[\varepsilon^2 + \Delta E \times \varepsilon + 2(H_{ac})^2] = 0$, and the resulting eigenvalues are $\varepsilon = 0$ and $\varepsilon_\pm \approx -\Delta E/2 \pm [\Delta E/2 - 2(H_{ac})^2/\Delta E]$ from Taylor's expansions; thus

$$H^s_{DA} = -\frac{\varepsilon_+}{2} = \frac{(H_{ac})^2}{\Delta E} \qquad \text{(A4)}$$

For the type B model of the $[(et\text{-}Fcpy)_2Ru(NH_3)_4]^{4+}$ ion in nitriles, the $\Delta G^\ddagger \approx 2500$ cm^{-1} between degenerate states ($\Delta G^\ddagger = \lambda/4$ in diabatic limit, where $\lambda \approx 10\,000$ cm^{-1}) is greater than the $\Delta G^\ddagger \approx 1400-1900$ cm^{-1} ($H_{ac} = H_{bc} \approx 400$ cm^{-1}) between the a and c states, and between the b and c states. Thus, the superexchange argument is that the charge delocalized onto the bridging state first and then delocalized onto another terminal. If $c \approx \sqrt{3}b/2$ (as a symmetric triangular case), the vertical energy (ΔE) upon position C is similar to $\lambda_a - \Delta G$ (ΔG in nitriles ranging between 900 and 1200 cm^{-1}). The H^s_{DA} calculated by eq A4 would approach 17−18 cm^{-1} when $H_{ac} \approx 400$ cm^{-1}.

(72) Bersuker, I. B. *Adv. Inorg. Chem.* **1992**, *81*, 703.
(73) Tsukerblat, B. S. *Group Theory in Chemistry and Spectroscopy*; Academic: London, 1994.

Supporting Information Available: CIF file; tables of crystal data for the [Fc−$(ph)_2$−Fc] complex; table of electrochemical and absorption data for the series of biferrocene complexes; ORTEP drawing of [Fc−$(ph)_2$−Fc] complex; absorption spectra of [(et-Fcpy)$Ru(NH_3)_5]^{3+}$, [(et-Fcpy)$Ru(NH_3)_4$(py)]$^{3+}$, [(et-Fcpy)$_2$Ru-$(NH_3)_4]^{3+}$ and of the series of biferrocene cations; Qualitative illustration of the two states for the solvent tunable and untunable states in PE plots. These materials are available free of charge via the Internet at http://pubs.acs.org.

IC801271Q